



**HAL**  
open science

## The shapes of dikes: Evidence for the influence of cooling and inelastic deformation

Katherine A. Daniels, Janine Kavanagh, Thierry Menand, R.S.J. Sparks

► **To cite this version:**

Katherine A. Daniels, Janine Kavanagh, Thierry Menand, R.S.J. Sparks. The shapes of dikes: Evidence for the influence of cooling and inelastic deformation. *Geological Society of America Bulletin*, 2012, 124 (7/8), pp.1102-1112. 10.1130/B30537.1 . hal-00720251

**HAL Id: hal-00720251**

**<https://hal.science/hal-00720251>**

Submitted on 16 Apr 2015

**HAL** is a multi-disciplinary open access archive for the deposit and dissemination of scientific research documents, whether they are published or not. The documents may come from teaching and research institutions in France or abroad, or from public or private research centers.

L'archive ouverte pluridisciplinaire **HAL**, est destinée au dépôt et à la diffusion de documents scientifiques de niveau recherche, publiés ou non, émanant des établissements d'enseignement et de recherche français ou étrangers, des laboratoires publics ou privés.

1 **The shapes of dikes: evidence for the influence of cooling and inelastic deformation.**

2 Katherine A. Daniels<sup>1</sup>, Janine L. Kavanagh<sup>2</sup>, Thierry Menand<sup>3,4,5</sup> and R. Stephen J. Sparks<sup>1</sup>.

3 <sup>1</sup>School of Earth Sciences, University of Bristol, Wills Memorial Building, Queen's Road,  
4 Bristol, BS8 1RJ, U.K.

5 <sup>2</sup>School of Geosciences, Monash University, Clayton Campus, Wellington Road, Clayton,  
6 Victoria, 3800, Australia.

7 <sup>3</sup>Clermont Université, Université Blaise Pascal, Laboratoire Magmas et Volcans, BP 10448, F-  
8 63000 Clermont-Ferrand, France.

9 <sup>4</sup>CNRS, UMR 6524, LMV, F-63038 Clermont-Ferrand, France.

10 <sup>5</sup>IRD, R 163, LMV, F-63038 Clermont-Ferrand, France.

11

12 **Abstract**

13 We document the shape of dikes from well exposed field locations in the Isle of Rum, Scotland,  
14 and Helam Mine, South Africa. The basaltic Rum dikes crop out on a smaller scale than the  
15 Helam kimberlite dikes and have a smaller length to thickness ratio (~100:1 Isle of Rum,  
16 ~1000:1 Helam Mine). We compare dike thickness field measurements with the geometry  
17 predicted by elastic theory, finding best-fit models to estimate magma overpressure and regional  
18 stress gradients at the time of dike emplacement. Most of the dike shapes fit poorly with elastic  
19 theory, being too **thick** at the dike ends and too narrow in the middle. Our calculated  
20 overpressures and stress gradients are much larger than independent estimates based on rock  
21 strength. Dike shape can be explained by a combination of host rock inelastic deformation and  
22 magma chilling at the dike's tapering edges preventing its closure as magma pressure declines

23 during emplacement. The permanent wedging of the dike edges due to chilling has implications  
24 for crustal magma transport and strain response in the crust due to dike emplacement.

25

## 26 **1. Introduction**

27 Dikes are the end result of the flow of pressurised magma through fractures, recording a  
28 fundamental mechanism of magma transport through the crust. Dike shapes reflect the  
29 integration of complex emplacement and eruption processes, [where](#) host-rock deformation,  
30 magma viscosity, magma pressure variations, stress distribution and heat transfer [all play a role](#).

31 Many theoretical and experimental studies of dike emplacement emphasize elastic deformation  
32 by pressurised magma-filled fractures (e.g. [Gudmundsson 1983](#), Lister and Kerr 1991, Kerr and  
33 Lister 1995, Rubin 1995, Menand and Tait 2001, Menand and Tait 2002, [Ray et al. 2007](#),  
34 Menand et al. 2010).

35

36 The shape of a preserved solidified dike can be used to calculate the pressure in the crack at the  
37 time of solidification, assuming that the shape reflects a simple elastic deformation control with  
38 fixed overpressure. Previous studies of dike shape have involved the measurement of dike  
39 thicknesses in the field and the observed dike cross-sectional profiles have been compared with  
40 elastic models in order to estimate the driving pressures and stress gradients at the time of  
41 emplacement (Pollard and Muller 1976, Delaney and Pollard 1981, Rubin and Pollard 1987,  
42 Poland et al. 2008, Geshi et al. 2010, [Kavanagh and Sparks, 2011](#)). Others have used theoretical  
43 numerical models to interpret the evolution of dike thickness. Buck et al. (2006) found that the  
44 stopping pressure of a dike (the point where the difference between the magma pressure and the  
45 tectonic stress (the driving pressure) at the dike tip becomes too small to [propagate](#) the dike) is

46 proportional to its thickness. They also found that the propagation distance is dependent on the  
47 initial distribution of tectonic stress and that dike intrusions affect the tectonic stress distribution,  
48 therefore affecting the propagation of subsequent dikes. Gudmundsson (2011) suggests that dike  
49 arrest is dependent on a number of factors including the size of the process zone (a region of  
50 highly fractured host-rock formed ahead of the propagating intrusion (see, for example, White et  
51 al., 2011)), in addition to the fracture toughness of both the host-rock itself and the interfaces  
52 between rock units. As a consequence, two dikes with the same overpressure could have quite  
53 different thicknesses.

54

55 We document the shapes of well exposed examples of basaltic dikes from the Isle of Rum,  
56 Scotland, and kimberlite dikes from Helam Mine, South Africa. Firstly we describe the  
57 geological settings of the dikes and present detailed dike-thickness datasets. We then summarize  
58 the theoretical framework used to assess to what extent elastic deformation can describe dike  
59 shape. We find that the shapes of most of the dikes have a poor fit with that expected from elastic  
60 theory and propose that the shapes can be explained by including the complicating effects of  
61 magma chilling at the dike's tapering edges and host-rock inelastic deformation.

62

63 Our observations have implications for understanding the development of dikes as conduits and  
64 for the effects of dikes on transient stresses and crustal strain. Through the permanent wedging  
65 open of the crust by chilled dike edges, a dike can act as a potential conduit for longer, increasing  
66 the longevity of eruptions. In addition the crustal strains implicit in dike emplacement reflect not  
67 only responses to tectonic stress but also magma overpressures preserved at the dike edges by  
68 chilling.

69

## 70 **2. Geological settings**

### 71 Basaltic dikes from the Isle of Rum

72 Situated off the west coast of Scotland, the Isle of Rum represents the eroded remnants of a  
73 shallow-level igneous complex emplaced into Torridonian Pre-Cambrian sandstone at  
74 approximately 2-3 km depth (e.g. Emeleus 1997, Nichols et al. 2009). Rum's igneous rocks  
75 include layered basic and ultrabasic intrusions, granophyres, volcanic rocks ranging from  
76 rhyolite to picrite, and hypabyssal intrusions (Emeleus 1997). The focus of this study is a late  
77 stage NW- to NNW-striking basaltic dike swarm (Emeleus 1997) dated to  $60.53 \pm 0.08$  Ma  
78 (Hamilton et al. 1998). The Isle of Rum and the dike measurement locations are shown in  
79 Figures 1A and B.

80

81 A dike length and thickness dataset was compiled. The length of each of the dikes selected was  
82 measured using a tape measure; **only dikes with crack tips exposed at both ends were selected for**  
83 **measurement**. The thickness of the dike was then measured at regular intervals. For the majority  
84 of the dikes, this was done by hand in the field. For a few of the largest dikes measured, this was  
85 done using scaled photographs. All measured thicknesses were then corrected for the dip angle  
86 of the dike to give the true thickness. A total of 1068 thickness measurements along the length of  
87 41 dikes are presented; some of these are **thought to be** en echelon segments of a single dike; **for**  
88 **simplicity we treat each segment individually as if they were separate dikes, referring to them as**  
89 **dikes rather than dike segments. We will address this simplification later on in the Discussion.**

90 The **Isle of Rum** dikes have a thickness:length ratio ranging from 1:11 to 1:449, with an average  
91 of 1:56. The measured lengths range between 0.08 and 47.6 m; the measured thicknesses range

92 between 0.007 m and 0.62 m with an average maximum thickness of 0.052 m. For most dikes the  
93 thickness measurements are accurate to about 2 mm. The largest dikes have thicknesses that are  
94 accurate to within 5 mm, and lengths that are accurate to the nearest 0.05 m. [The smallest dikes](#)  
95 [are likely to be part of a segmented dike, or offshoots from a larger dike, and are not expected to](#)  
96 [have travelled far](#). The dikes intruded contact metamorphosed Torridonian Sandstone. Most  
97 dikes show pronounced chilled margins of at least a few millimeters (Figure 2A) and many show  
98 internal cooling fractures (Figure 2B). Many Rum dikes exhibit crack tip infilling with sediment  
99 (Figure 2A) and some show branching. Most dikes cross-cut pre-existing bedding and joints, or  
100 are themselves affected by post-emplacement jointing (Figure 2B). Few dikes have joint  
101 controlled orientations (Figure 2C) and those affected by a previous joint set were not included  
102 in the analysis. Occasional host rock inclusions are seen (Figure 2B).

103

#### 104 The Swartruggens Kimberlite Dike Swarm

105 The Swartruggens Kimberlite Dike Swarm, Helam Mine, South Africa, comprises three dikes;  
106 two kimberlites (Main and Changehouse dikes) and a lamprophyre (Muil dike). The dikes  
107 intruded at the end of the Jurassic ([Allsopp and Barrett, 1975](#); [Phillips, 1991](#); Gurney and  
108 Kirkley 1996), and cut a stratigraphy comprising dolerite, quartzite, shale and andesite lava from  
109 the Proterozoic Pretoria Group, central Kaapvaal craton. The estimated magma emplacement  
110 depth is 2-3 km (Brown et al. 2007). Mine excavations extend to 750 m deep and give a three-  
111 dimensional view of the structure of [the](#) kimberlite dikes. A unique dataset of 683 dike-thickness  
112 measurements from Levels 16-21 of John's dike segment, and 704 dike thickness measurements  
113 from Levels 19-22 of Edward's dike segment are presented. The measurements were made by  
114 hand using a tape measure [by a number of geologists systematically since the mine has been](#)

115 active. A simplified diagram of the field relationships of these dike segments is shown in Figures  
116 3A and B.

117

118 The Main dike comprises a series of anastomosing en echelon segments extending 7 km (Basson  
119 and Viola 2003). The dike segments trend approximately east-west with a thickness:length ratio  
120 of ~1:1000; each segment strikes approximately 1 km in length with a mean thickness of 0.64 m  
121 (Kavanagh 2010; Kavanagh and Sparks, 2011). The measurements made of dike thickness are  
122 accurate to the nearest 0.05 m. The lateral extent of the mined excavation is used as a proxy for  
123 the breadth of the dike as this closely follows the dike geometry; the errors associated with this  
124 measurement are estimated at less than 10 meters. Breccia zones up to several tens of meters  
125 wide occur in the regions between dike segments, where centimeter-sized angular country rock  
126 fragments have formed (Brown et al. 2007). These fragments occur as inclusions within the  
127 kimberlite. Spheroidally weathered dolerite is associated with breccia zones and centimeter-thick  
128 dike-parallel fracture zones that occur in the host rock at the dike margins (Brown et al. 2007).  
129 The country rock away from the dike is unbrecciated, lacking closely spaced fracturing and  
130 spheroidal weathering.

131 The Swartruggens dikes are not thought to be controlled by pre-existing fractures, having instead  
132 created and intruded their own fractures during ascent. The host rock is jointed with no dominant  
133 orientation, is brecciated especially near the fracture tips, and there is evidence for stoping  
134 (Brown et al. 2007). Chilled margins were not recognized in the Swartruggens dikes; they likely  
135 existed but are obscured by post-emplacement serpentization. Closely-spaced host rock  
136 fracturing, predominantly sub-parallel to the dike contact, is pervasive in the vicinity (0.1 to 1 m)  
137 of the Swartruggens dike margins.

138

### 139 **3. Theoretical framework and comparison with field data**

140 Elasticity theory (e.g. Timoshenko and Goodier 1970, Landau and Lifshitz 1986) describes the  
141 two-dimensional shape of a fluid-filled fracture subjected to a stress field in a homogenous and  
142 isotropic material (Sneddon 1946, Pollard and Muller 1976):

143

$$144 \quad u_y = \frac{l \sin \theta}{2G} [(P_o - S_{y_o})(1 - \nu)] = \frac{l \sin \theta}{2G} [(\Delta P)(1 - \nu)] \equiv A \sin \theta \quad (1)$$

145

$$146 \quad u_y = \frac{l^2 \sin 2\theta}{16G} [(\nabla P - \nabla S_y)(1 - \nu)] \equiv B \sin 2\theta \quad (2)$$

147

148 where  $l$  and  $u_y$  are the crack length and displacement,  $\theta$  is the angular position along the slit from  
149 the crack centre,  $G$  is the elastic shear modulus,  $P_o$  and  $S_{y_o}$  are the magma pressure and regional  
150 stress normal to the crack,  $\Delta P$  is the excess magma pressure  $P_o - S_{y_o}$ ,  $\nu$  is the host rock's Poisson's  
151 ratio,  $\nabla P$  is the magma pressure gradient along the crack,  $\nabla S_y$  is the regional normal stress  
152 gradient along the crack, and A and B are constants. Model parameter values are given in the  
153 caption to Figure 4.

154

155 The overall displacement of the margins of the fluid filled crack is the result of a summation of  
156 both Equations (1) and (2). Equation (1) gives the displacement due to the application of a  
157 uniform internal pressure with no gradient in regional stress, whilst Equation (2) gives the  
158 displacement as a result of a linear gradient along the dike length as the difference between the  
159 regional stress and magma pressure. Models including a constant driving pressure plus a gradient  
160 in driving pressure or regional stress along the dike length will create a dike profile with a

161 teardrop shape (Pollard 1987). Asymmetrical dike profiles have been attributed to gradients in  
162 magma pressure or regional stress with the magnitude of asymmetry being controlled by the  
163 length of fracture, overpressure and effective stress gradient (Pollard and Muller 1976).

164

165 We analyze dike-thickness measurements from the two datasets using the method of Pollard and  
166 Muller (1976). Equations (1) and (2) were iterated through 10,000 permutations of A and B to  
167 estimate the best parameter values that minimize the least squares misfit between the model and  
168 the observations. Overpressures and linear stress gradients are estimated from the best-fit  
169 models. The estimated values of overpressure and linear stress gradient are then used as a  
170 reference for comparison with the field data. These equations have been used to generate a model  
171 to fit the shape of an observed solidified magma filled crack. By interpreting the static shape, the  
172 assumption has been made that the fluid filled crack had reached a static equilibrium and that  
173 flow effects as solidification occurred can be neglected.

174

#### 175 **4. The shapes and thicknesses of the dikes**

176 Figure 4 shows examples of representative dike profiles for Rum and Swartruggens as horizontal  
177 cross-sectional slices. It is assumed that the cross-sectional profile of the dikes at each field  
178 locality is approximately horizontal. The best fitting elastic model is shown as the solid black  
179 line. Overpressures estimated from the models range from 37-1990 MPa, averaging 678 MPa  
180 ( $R^2=0.389-0.997$ , average=0.921) for Rum, and from 4-40 MPa ( $R^2=0.50-0.72$ ) for Swartruggens  
181 (Table 1). Estimated regional stress gradients for the Rum dikes estimated from the theory are up  
182 to  $3 \text{ GPa m}^{-1}$ , averaging  $622 \text{ MPa m}^{-1}$ , and range from  $15-87 \text{ kPa m}^{-1}$  for Swartruggens (Table 1).

183 A comparison of the values of overpressure and stress gradient estimated for the Rum and  
184 Swartruggens dikes with values obtained by previous studies are also given in Table 1.

185

186 The range of  $R^2$  values for the best-fit models indicate that many of the dike segments do not fit  
187 the elastic model well. In Figure 4 the data have been normalised ( $L^*$ ) to the overall length of  
188 each dike giving the tips at -0.5 and +0.5. This normalization procedure allows us to compare the  
189 dikes of different length scales, and to compare all the data with the elastic model in one  
190 diagram.

191

192 In Figures 5A) to D), all thickness measurements have been referenced to the model fit which is  
193 plotted as a horizontal line in the normalised co-ordinates to show departures in dike thickness  
194 from the model. Figures 5C) and D) show the same graphs as Figures 5A) and B) but with a  
195 larger scale on the y-axis. Negative y-axis values indicate a dike which is **thicker** than predicted  
196 by the model, while positive values show a dike that is thinner than predicted. Frequency  
197 histograms of the difference between the modelled thickness and the measured thickness for the  
198 Rum and Swartruggens dikes are shown in Figures 5E) and F), respectively. For both localities,  
199 the distribution of the data from the central portions of the dikes ( $L^* = -0.3$  to  $0.3$ ; **red bars**) is  
200 positively offset from 0 on the x-axis whilst the distribution of the data from the edge portions of  
201 the dikes ( $L^* < -0.3$  and  $> 0.3$ ; **black bars**) is negatively offset from 0 on the x-axis. The **mean**  
202 average difference between the model and the measured data in the central portion is 0.11 for the  
203 Rum data, and 0.02 for the Swartruggens data, whilst for the edges the difference is -0.10 for the  
204 Rum data and -0.29 for the Swartruggens data. The Rum and Swartruggens dikes both show,

205 irrespective of goodness of fit, that dikes strongly tend to be thicker than expected by the model  
206 at their edges and thinner than expected in their centers.

207

208 [Our data shows](#) dike segments are commonly asymmetrical about their length mid-point. In plan-  
209 view, the Swartruggens dikes and many Rum dikes are skewed so the point of maximum  
210 thickness is not at the dike centre ([e.g.](#) Figure 4B). We have quantified dike asymmetry ( $\delta$ ) by  
211 comparing the best-fit model centre with the dike's normalized length mid-point: a  $\delta$  of 0 is  
212 symmetrical and 0.5 is maximum possible asymmetry. For the Rum dikes,  $\delta$  ranges from 0-0.47  
213 (average 0.142, standard deviation (s.d.) 0.110), for the Swartruggens dike John segment  $\delta$   
214 ranges from 0.087-0.203 (average 0.154, s.d. 0.054), and from 0.179-0.242 (average 0.205, s.d.  
215 0.031) for the Edward segment. The Rum dikes have a broader range of  $\delta$  values; some dikes  
216 show extreme asymmetry. The Swartruggens dikes are more skewed than the Rum dikes with  
217 less variation in  $\delta$ . We found no correlation between asymmetry and dike size. Neighbouring  
218 segments commonly show asymmetry in alternating directions which may be the result of  
219 compression as one dike segment influences the next one ([e.g. Pollard et al. 1982](#), Roman and  
220 Cashman 2006).

221

## 222 **5. Discussion**

223 [We first discuss dike segmentation and our simplified analysis, before discussing](#) the two kinds  
224 of mismatch [we found](#) between the elastic theory and the observations: estimated overpressure  
225 and stress gradient values are implausibly high, [and](#) dikes are systematically thicker at the edges  
226 and thinner in the middle.

227

## 228 Segmented dikes

229 Some of the dikes measured on Rum are individual dikes (4) (Figure 6A) whilst others are  
230 segments of a larger dike (37) (Figure 6B). The Swartruggens dikes are segments of a larger  
231 regional intrusion. Previous workers have treated segmented dikes both as individual intrusions  
232 or have modelled the segments together as one intrusion (e.g. Pollard and Muller 1976, Delaney  
233 and Pollard 1981, Baer 1991 and Poland et al. 2008). Dike segmentation commonly occurs in  
234 response to stress field rotation or propagation at an angle to the principal stress directions,  
235 giving a series of en echelon dike fingers, or segments, with systematic step-overs between  
236 segments owing to tangential stress on the dike walls (Pollard 1987). Segmentation may also  
237 reflect dike propagation through heterogeneous geological media with local deviations of the  
238 stress field. The Swartruggens dikes and most of the Rum dikes are better interpreted with the  
239 latter explanation as the segments step direction is non-systematic. Segmentation implies a more  
240 complicated local stress regime than a static elastic theory based on a fluid filled crack and these  
241 complications are not easily qualified. Indeed the correct mathematical treatment of this complex  
242 problem requires knowledge of the principal directions, principal stresses and magma  
243 overpressure distribution along the fluid-filled crack (Meriaux and Lister, 2002); *a priori*  
244 estimates based solely on dike orientations can lead to significant errors in the principal stress  
245 values (Meriaux and Lister, 2002), and thus the quantification of dike segmentation.

246

247 Additionally, we note some difficulties in treating a dike with several segments as a single dike.  
248 Although in some cases this can provide a better fit to the thickness data (e.g. Delaney and  
249 Pollard 1981, Poland et al. 2008), especially if the thickness close to the tips is not measured, the  
250 quality of the fit inherently depends on the amount of data and their position along each segment.

251 Our dike thickness measurements have a high frequency, including measurements made at the  
 252 segment tips. As the thickness decreases to zero at the tips, this cannot be properly fit by a single  
 253 opening curve for a set of segments. In addition, the true lateral extend of a segmented dike is  
 254 rarely known for certain. Yet, this information is crucial as it constrains the overpressure  
 255 estimate: all else being equal, a larger dike length will provide a lower overpressure estimate to  
 256 explain the observed dike thickness.

257

258 A simplified static analysis whereby a segmented dike is represented by a series of collinear,  
 259 identical and equally spaced segments with the same overpressure  $\Delta P$  allows the opening  $u_s$  of  
 260 the segments along their length  $2a$  to be calculated analytically as a function of their  
 261 overpressure, length and spacing (Tada et al. 2000, Gudmundsson 2011):

$$262 \quad u_s = \frac{2\Delta P(1-\nu)}{\pi G} a(1+s) \left\{ \ln \left[ \cos \left( \frac{\pi x}{2(1+s)} \right) + \sqrt{\cos^2 \left( \frac{\pi x}{2(1+s)} \right) - \cos^2 \left( \frac{\pi}{2(1+s)} \right)} \right] - \ln \left[ \cos \left( \frac{\pi}{2(1+s)} \right) \right] \right\}. \quad (3)$$

263  $\nu$  is the host-rock Poisson's ratio,  $G$  its shear modulus, and the tip-to-tip distance  $d$  between  
 264 adjacent dike segments is normalised to the segment length:  $s = d/2a$ . Figure 7 shows how much  
 265 the opening of multiple segments differs from that of a single one with the same overpressure.  
 266 Closer dike segments have greater openings, but even for dike segments separated by 1/1000 of  
 267 their length this opening is increased only by a factor of less than five (Figure 7B). The segment  
 268 openings are proportional to their overpressure, and consequently this simplified analysis  
 269 suggests that, by considering each segment separately, the overpressure is overestimated by a  
 270 factor of about five. A more robust analysis would consider the relative positions of observed  
 271 segments, but this would require a numerical treatment. However, the contribution of segments  
 272 with larger spacing would be lower, and could offset some of the closest segments.

273

274 To investigate further the effect of analyzing dike segments collectively rather than separately,  
275 we have compared this analysis with the profile of six en echelon dikes from one locality on the  
276 Isle of Rum. The dikes at this particular locality are thought to be a completely exposed  
277 segmented dike; at all other localities where the dikes were segmented the complete extent of the  
278 dike is less certain. These six dike segments are not truly collinear, however. There is always  
279 some separation, as measured normal to one segment, and they also tend to overlap, with both  
280 separation and overlap distances varying significantly from a pair of segments to one another.  
281 We have thus used the collinear, segmented dyke analysis with a range of tip-to-tip spacing  
282 between segments, from 1 m down to 0.1 mm. As for the previous analysis, equation (3) was  
283 iterated through 1000 permutations of  $\Delta P$  to estimate the best overpressure value that minimizes  
284 the least squares misfit between equation (3) and the measured opening for each segments. The  
285 best overpressure estimates range from 73 MPa to 1906 MPa with an averaged estimate of 430  
286 MPa. The highest estimate, found for only one of the six segments, is an order of magnitude  
287 higher than the other five estimates; adjacent segments belonging to the same dike should have  
288 similar overpressures. Neglecting this highest value gives an average overpressure estimate of  
289 135 MPa. Although these values are lower than those estimated with Pollard and Muller's  
290 analysis, the best overpressure estimates predicted by the segment analysis are still much higher  
291 than values documented in previous studies (Table 1). Figure 8 shows the best-fit profiles for  
292 both single-dyke and segmented-dyke analyses for two of the selected segments. Both analyses  
293 fail to explain the thick edges displayed by the segments (Figure 8A). Additionally, the segment  
294 analysis only deals with constant stress, and so cannot say anything about regional stress  
295 gradients nor explain the asymmetrical, teardrop shape displayed by most segments (Figure 8B).

296

297 Finally, several of the Rum segments overlap. We are not aware of any analytical solution for  
298 estimating overpressures, stress gradients or shape for overlapping segments; this would require  
299 numerical computations. Considering a constant overpressure, Pollard et al. (1982) showed that  
300 overlapping segmented dikes would be fatter than a single one. So by considering each segment  
301 as an individual dike, one would overestimate its overpressure. This overestimation will increase  
302 with the number of segments that constitute a whole dike, but will decrease for increasingly  
303 overlapping segments and higher rotation angle between the segment direction and that of the  
304 main dyke (Pollard et al., 1982). Overlapping segments will also tend to induce segment  
305 asymmetry as well as pinching or thinning of the edges (Pollard et al. 1982). This could  
306 potentially explain the extremely high stress gradients derived from Pollard and Muller's analysis  
307 as well as some of the pinched segment profiles. However this cannot explain the overall,  
308 general shape pattern displayed by both the Rum and Swartruggens dikes: all these dikes appear  
309 fatter at their edges than predicted by both Pollard and Muller's and the segmented analyses, and  
310 they would appear even fatter for overlapping, pinching segments.

311

312 Considering all these limitations and effects together, it seems our single dike analysis would  
313 overestimate overpressures by at most a factor 10, and appears to be the best analytical method  
314 for fitting the measured profiles. Therefore, treating each segment as an individual dike provides  
315 a fairer assessment of their overpressure, stress gradient and shape.

316

317 Overpressure and stress gradients

318 The elastic model of Pollard and Muller (1976) fits the data poorly for most of our studied dikes.  
319 The first mismatch between the data and the elastic model is the calculated values of  
320 overpressure and stress gradient which are very large. This is evident from the comparison with  
321 the values estimated in previous studies (Table 1) (Geshi et al. 2010, Poland et al. 2008, Pollard  
322 and Muller 1976). The overpressures are especially large and likely unphysical for the Rum  
323 dikes, while the Swartruggens dikes' values are large but more plausible. The stress and  
324 overpressure gradients calculated are mostly implausible for both examples. If the Rum dikes  
325 with lengths < 1 m are neglected, the range of estimated overpressure values is unchanged (37 –  
326 1990 MPa), although the average is slightly reduced to 398 MPa. If the Rum dikes with  
327 thicknesses < 0.05 m are neglected, the estimated values of overpressure are 70 – 1990 MPa,  
328 averaging 710 MPa. There appears therefore to be no dependence of these results on dike size.  
329 One could reduce these overpressure and stress gradient estimates by up to an order of  
330 magnitude if we consider each dyke individually and not as segments from a larger dike (see  
331 previous section). Yet the majority of these estimates remain much higher than values reported in  
332 previous studies (Table 1).

333

334 Very high values of overpressures and stress gradients cannot be explained using an elastic  
335 model. A rock's tensile and compressive strengths are typically of order 10 MPa and 50 MPa  
336 respectively, whilst magma overpressures have been estimated at <20 MPa (Stasiuk et al. 1993,  
337 Gudmundsson 1999). For a 20 MPa magma source overpressure (the magma pressure in excess  
338 of the regional, compressive tectonic stress), a dike propagating 1 km from its source would  
339 experience a regional stress gradient of  $\leq 20$  kPa m<sup>-1</sup> (Jaupart and Allegre 1991) and this stress  
340 gradient estimate would decrease as the dike propagates further from its source. A dike driven by

341 buoyancy would have a driving stress gradient of  $\Delta\rho g$ , where  $\Delta\rho$  is the density difference  
342 between the magma and the host rocks and  $g$  is the gravitational acceleration. A magma-host  
343 density difference of  $100 \text{ kg m}^{-3}$  gives a stress gradient of only  $1 \text{ kPa m}^{-1}$ . Stress gradients as high  
344 as those estimated for the Rum and Swartruggens dikes would therefore necessitate magma  
345 buoyancies greatly in excess of natural values governed by density differences between magmas  
346 and host rocks.

347

348 The fracture toughness of a rock is important in terms of the dike opening. According to Linear  
349 Elastic Fracture Mechanics, the intrusion of magma into a rock requires the concentration of  
350 stress at the intrusion tip to exceed the fracture toughness  $K_c$  of that rock (Pollard, 1987). This is  
351 equivalent to having an overpressure greater than  $\sim K_c/(L)^{1/2}$ , where  $L$  is the length of the  
352 magma-filled crack. Rocks with higher fracture toughness both require higher magma  
353 overpressure for the dikes to propagate and induce greater blunting of the dikes at their tip.  
354 Laboratory measurements of fracture toughness give values on the order of  $1\text{-}10 \text{ MPa m}^{1/2}$ , and so  
355 kilometer-long dikes would be expected to propagate with overpressures of  $1 \text{ MPa}$ . Larger dikes  
356 would require even lower overpressures. Conversely, our estimated overpressures would suggest  
357 rock fracture toughness of the order  $10\text{-}10^4 \text{ MPa m}^{1/2}$  and  $10^2\text{-}10^3 \text{ MPa m}^{1/2}$  for the Rum and  
358 Swartruggens dikes, respectively. These are much higher values than measured in the laboratory  
359 (e.g. Schmidt and Huddle, 1977), but similar to other field-based fracture toughness estimates  
360 (Delaney and Pollard, 1981; Delaney et al., 1986; Reches and Fink, 1988, Gudmundsson 2009).  
361 Such high values are either explained by large confining pressures at the time of dike intrusions  
362 or extensive inelastic deformation ahead and around the dike tip (Delaney et al., 1986; Rubin,  
363 1993; Fialko and Rubin, 1997). The former explanation would necessitate depths of intrusion

364 greater than that of the Rum and Swartruggens dikes, whilst the latter explanation is plausible but  
365 requires extensive inelastic deformation.

366

367 Various non-elastic explanations could be invoked to explain the high estimated [overpressure](#)  
368 [and stress gradient](#) values. If the elastic parameter values used in the model were too large, the  
369 overpressures and stress gradients would be overestimated. Dikes may form through the dilation  
370 of pre-existing fractures that are suitably orientated with regards to principal stress directions  
371 (e.g. Gudmundsson 1984, Delaney et al. 1986, Valentine and Krogh 2006), reducing the [stress](#)  
372 required to fracture the host-rock. Once a fracture [is re-sealed](#), the probability of a fracture  
373 reinitiating in the same location is greater ([the host-rock's compliance](#)) and the shear modulus of  
374 the rock can be reduced by a factor of 2 or 3 (Worthington and Lubbe 2007, Kavanagh 2010),  
375 [effectively making the crust less rigid](#). For the Rum dikes [showing](#) evidence of intruding host-  
376 rocks with many pre-existing joints, the compliance may have been significant. The opening of a  
377 dike is linearly proportional to its overpressure and inversely proportional to the shear modulus  
378 of the host rocks (e.g. Pollard, 1987). Therefore, accounting for the compliance can only partly  
379 explain the large overpressures estimated for the Rum dikes; typical changes in elastic properties  
380 due to compliance would only alter the calculated values by about a factor of 3 in the Rum and  
381 Swartruggens cases.

382

383 Magma extrusion from a greatly pressurised chamber into surrounding rock also provides an  
384 explanation for high calculated overpressures, particularly on Rum. [Magma chamber](#)  
385 [overpressure increases](#) during edifice growth until edifice destruction occurs (Pinel and Jaupart  
386 2000, Pinel and Jaupart 2003, Pinel and Jaupart 2004). The Rum dikes may represent magma

387 extrusion from a chamber during the [high-overpressure edifice-building](#) stage. Typical  
388 stratovolcanic cones exert a load of approximately 50 MPa, significantly affecting the rock  
389 stresses beneath the volcanic edifice (Pinel and Jaupart 2003). Edifice size strongly affects the  
390 critical magma overpressure required for eruption, [which](#) may be much larger than the host-rock  
391 tensile strength (Pinel and Jaupart 2003). This is a more plausible model for explaining some of  
392 the overpressures calculated for the Rum dikes as a volcanic edifice was present at the time of  
393 diking.

394

395 High overpressures may also be partly attributed to shear failure. Assuming a shear component is  
396 present whilst diking occurs, dikes may tend to be wider than otherwise expected, leading to  
397 higher calculated overpressures. [A shear](#) component could be caused along the dike length if  
398 [intrusion occurs](#) in an orientation divergent from  $\sigma_1$ , as would be likely when intruding pre-  
399 existing joints. This is consistent with the offset and overlapping dike segment pattern commonly  
400 seen on Rum, [suggesting](#) propagation along non-principal stress directions.

401

402 Both Rum and Swartuggens dikes give very high calculated stress gradient values, much larger  
403 than the values estimated from previous studies (Table 1). Assuming constant elastic properties  
404 and local horizontal magma pressure, the calculated stress gradients represent mainly horizontal  
405 gradients in crustal stress. Taking a calculated stress gradient value of 65 kPa m<sup>-1</sup> for a  
406 Swartuggens dike, the crustal stress normal to the dike would change by 65 MPa over a 1 km  
407 region, an implausibly large horizontal value in the upper crust. This stress gradient would  
408 require a surface topography change of about 3 km, which is unlikely in this region of southern

409 Africa. The Rum dikes give calculated stress gradients that are two orders of magnitude larger;  
410 even with very strong lateral stress gradients, these values are extremely large.

411

412 A lateral variation in host rock properties has also been invoked in order to explain stress  
413 gradient values (e.g. Pollard and Muller 1976, Kavanagh and Sparks 2011) as well as variations  
414 in dike thickness (e.g. Baer 1991, Geshi et al. 2010). This is unlikely to be the cause of the high  
415 stress gradients estimated for the Rum dikes as these intruded within one rock unit; variations in  
416 burial depth along their strike would also be too small to have a significant effect.  
417 Heterogeneities in the sandstone layers may add to the variations in dike thickness of the Rum  
418 dikes. However, the majority have a small enough scale that even the properties of the single  
419 rock unit are unlikely to have changed significantly. Variable host rock properties are thus  
420 unlikely to have caused the thickness variations or the stress gradient values measured on Rum.

421

422 The cause of the dike asymmetry is most likely due to host-rock inelasticity, small scale lateral  
423 host-rock property variations, and most importantly, the interference of dike edges and  
424 overlapping segments. Successive emplacement of neighbouring dikes and dike segments will  
425 alter the stress distribution in the host rock (e.g. Rubin and Pollard 1987). Overlapping segments  
426 with solidified magma pinning the dike edges in position is the likely cause of the asymmetry  
427 seen.

428

429 The dike shape

430 Changing the elastic parameters in the model does not improve the overall fit because of the  
431 mismatch between the predicted and observed dike shape. The modelled dike thickness is

432 overestimated at the centre and mostly underestimated at the edges (Figure 5). Most of the dikes  
433 measured had a flatter central section than predicted. An active dike's width is determined by the  
434 overpressure which usually declines with time as the chamber pressure decreases, manifest by  
435 waning flow rate in many lava eruptions (Stasiuk et al. 1993), although the thickness can also be  
436 determined by the dike length for a fixed overpressure. If a dike erupts, this dike and the overall,  
437 not-yet-solidified, intrusive system will experience a reduction in overpressure. However, the  
438 majority of dikes are not thought to erupt (e.g. Gudmundsson 1984, Gudmundsson et al. 1999).  
439 Arrested dikes can still however experience a reduction in overpressure during intrusion. At  
440 neither of the studied field localities were we able to find unequivocal field evidence of the  
441 magma transport direction; these may therefore have propagated vertically or laterally. For a  
442 constant magma volume, provided that the crack is not buoyancy driven, the overpressure in an  
443 intruding crack will decrease as the length of the crack increases (McLeod and Tait 1999).  
444 Moreover, however the intrusion is driven, its overpressure will decrease because of the viscous  
445 pressure drop it will experience during propagation (Lister and Kerr, 1991). We do not see direct  
446 evidence that the dikes from either locality connected to their palaeosurface, and therefore we  
447 must rely on indirect evidence to assess whether or not these dikes were feeders. If it can be  
448 assumed that at tens of meters depth a dike with a maximum thickness greater than one meter has  
449 the potential to act as a feeder dike (Geshi et al. 2010), the Swartruggens dike segments (which  
450 have a maximum thickness of 1.95 meters; Kavanagh and Sparks, 2011) could potentially have  
451 acted as feeder dikes. As the mean thickness of the dikes measured at both field locations is less  
452 than one meter, it is assumed that our analysis can only be applied to dikes fulfilling this  
453 criterion, and the application of our results to thicker dikes will require further investigation.

454

455 As magma flows through a fracture (Figure 9A), chilling of the magma at the dike margins  
456 prevents it from closing at the tips (Figure 9B). Viscosity increase by preferential cooling at the  
457 dike edges adds to this effect. As the overpressure wanes, if the position of the edges becomes  
458 fixed and the dike is no longer propagating in the direction of the tip, the preserved thickness is  
459 then determined by the initial overpressure (Figure 9C). However, the non-solid and less viscous  
460 central parts of the dike can close as the overpressure declines; the initial dike injection shape is  
461 not the shape that is ultimately preserved as the solidified dike. We suggest therefore that the  
462 shape mismatch is principally a result of chilling and solidification during dike emplacement.

463

464 Inelasticity can also account for some of the dike thickness variation. There is strong evidence  
465 for inelastic deformation in the zones between the Swartruggens dike segments, which may have  
466 reduced the host-rock rigidity and shear strength. Mechanical processes such as brecciation,  
467 stoping and weathering (preferentially focused at dike termination points, over-laps and relay  
468 zones) can weaken the rocks prior to magma emplacement and produce an inelastic host-rock  
469 response during emplacement (Brown et al. 2007, Kavanagh 2010, Kavanagh and Sparks, 2011).  
470 Similar inelastic deformation between adjacent segments has been observed by Schofield et al.  
471 (2010) at the Golden Valley Sill, South Africa. Additionally, small segments such as those  
472 observed on Rum are likely to correspond to segments lying close to the very tip of their main  
473 dike, and so to be embedded within the inelastic, damaged region that surrounds that main dyke  
474 tip. Indeed, the size of this damage region tends to scale with that of the dyke that created it  
475 (Faulkner et al., 2011), and could reach several meters or tens of meters (e.g. Delaney et al.,  
476 1986). Inelastic deformation within the damage zone would contribute to blunting the edges of  
477 the segments embedded there. Thus inelastic deformation could both explain the apparent high

478 values of rock fracture toughness, suggested by our high overpressure estimates, and the  
479 observations of dike tips that are thicker than expected from elastic theory. Inelastic deformation  
480 in the steps between segments also provides an explanation for those dikes which are markedly  
481 asymmetric. Much more inelastic deformation at one end of the dike than the other will mean a  
482 distortion of the shape that results in asymmetry. The observation of alternations in the sense of  
483 asymmetry of segments indicates too that complex inelastic deformation in the step-over regions  
484 has occurred.

485

#### 486 Implications for eruption longevity and crustal strain

487 The tendency for [thick dike tips](#) and narrow centers has broader implications. The wedging of the  
488 dike edges formed at high magma overpressures is made permanent by chilling. Thus as the  
489 pressure reduces and the eruption wanes, the fracture will be prevented from closing fully and  
490 the dike can continue to act as an open conduit for longer than it otherwise would have been able  
491 to. Dike emplacement can be regarded as the accommodation of crustal strain as a response to  
492 tectonic stresses. However, the dimensions of an active dike with magma pressures exceeding  
493 tectonic stresses indicate that the transient strain can exceed the tectonic strain expected. Since  
494 the now chilled edges have previously been pushed apart under a high magma overpressure, the  
495 additional strain can be permanently preserved due to the chilled and wedged dike edges. For  
496 large dikes with prolonged flow at overpressures exceeding tectonic stresses and with substantial  
497 solidification along the dike edges the excess strain could be substantial.

498

#### 499 7. Conclusions

500 Many of the dikes measured on Rum and at Helam Mine are poorly fit by the classical elastic  
501 model of Pollard and Muller (1976). There are two distinct mismatches between the presented  
502 data and the elastic model. Firstly, many dike shapes are too thin in the middle and too **thick** at  
503 the edges to be fit by an elastic profile; the calculated  $R^2$  values range from 0.389-0.997 and the  
504 misfits are larger than measurement uncertainties. Secondly, even for dikes where the model fit  
505 is acceptable, the calculated magma driving pressures and linear stress gradients are very large,  
506 particularly for the small-scale basaltic dikes on Rum. Many explanations have been provided to  
507 account for the differences. Of these, the cooling of the dike edges wedging the fracture open,  
508 and the host-rock inelastic deformation pre- and syn- **magma** emplacement provide the most  
509 complete explanation for the mismatches between the data and the model. **Care should be taken**  
510 **when extrapolating the observations from the dikes measured from the Swartruggens swarm and**  
511 **on Rum. As the mean observed dike thickness was less than a meter, it is not automatic to**  
512 **assume that the analysis will apply to larger dikes; the application of the results to thicker dikes**  
513 **will require further investigation.**

514

#### 515 **Acknowledgements**

516 KAD would like to thank R. C. Ogilvie-Harris for assistance with the Rum data collection. **A.**  
517 **Gudmundsson, A. E. L. Ferrari and an anonymous reviewer are gratefully acknowledged for**  
518 **providing valuable comments to improve the manuscript.** M. Poland and two anonymous  
519 reviewers are thanked for helpful comments on an earlier shorter form of the manuscript. **J.**  
520 **Davidson and A. Rogers are thanked for permission to publish the dataset from Helam Mine.**  
521 RSJS, JLK and TM were supported by a grant from the Leverhulme Trust. RSJS is co-supported

522 by an advanced grant from the European Research Council. KAD was supported by a NERC

523 Consortium Grant.

524

525

526 **References**

527 [Allsopp, H.L. & Barrett, D.R. 1975. Rb–Sr age determinations on South African kimberlite](#)  
528 [pipes. \*Physics and Chemistry of the Earth\*, 9, 605–617.](#)

529 Baer, G., 1991. Mechanisms of dike propagation in layered rocks and in massive, porous  
530 sedimentary rocks. *Journal of Geophysical Research* 96, 11911-11929.

531 Basson, I. J., and Viola, G., 2003. Structural overview of selected Group II kimberlite dyke  
532 arrays in South Africa: implications for kimberlite emplacement mechanisms. *South African*  
533 *Journal of Geology* 106 (4), 375 - 394.

534 Brown, R. J., Kavanagh, J. L., Sparks, R. S. J., Tait, M., and Field, M., 2007. Mechanically  
535 disrupted and chemically weakened zones in segmented dike systems cause vent localization:  
536 Evidence from kimberlite volcanic systems. *Geology* 35 (9), 815 - 818.

537 Buck, W. R., Einarsson, P., and Brandsdottir, B., 2006, Tectonic stress and magma chamber size  
538 as controls on dike propagation: constraints from the 1975-1984 Krafla rifting episode: *Journal of*  
539 *Geophysical Research*, v. 111, doi:10.1029/2005JB003879.

540 Delaney, P. T., and Pollard, D. D., 1981. Deformation of host rocks and flow of magma during  
541 growth of Minette dikes and breccias-bearing intrusions near Ship Rock, New Mexico. U. S.  
542 Geological Survey professional paper 1202.

543 Delaney, P. T., Pollard, D. D., Ziony, J. I., and McKee, E. H., 1986. Field relations between  
544 dykes and joints' emplacement processes and paleostress analysis. *Journal of Geophysical*  
545 *Research* 91 (B5), 4920 - 4938.

546 Domenico, S. N., 1983. Sandstone and limestone porosity determination from shear and  
547 compressional wave velocity. *Bulletin of the Australian Society of Exploration Geophysicists* 14  
548 (4), 81 - 90.

549 Emeleus, C. H., 1997. Geology of Rum and the adjacent islands. British Geological Survey  
550 Memoir for 1:50 000 Geological Sheet 60 (Scotland). The Stationery Office.

551 [Faulkner, D. R., Mitchell, T. M., Jensen, E., and Cembrano, J., 2011. Scaling of fault damage](#)  
552 [zones with displacement and the implications for fault growth processes. Journal of Geophysical](#)  
553 [Research 116, B05403, doi:10.1029/2010JB007788.](#)

554 Fialko, Y. A., and Rubin, A. M., 1997. Numerical simulation of high-pressure rock tensile  
555 fracture experiments: evidence of an increase in fracture energy with pressure? Journal of  
556 Geophysical Research 102 (B3), 5231 – 5242.

557 Geshi, N., Kusumoto, S., and Gudmundsson, A., 2010. Geometric difference between non-feeder  
558 and feeder dikes. Geology 38 (3), 195-198.

559 [Gudmundsson, A., 1983. Form and dimensions of dykes in Eastern Iceland. Tectonophysics 95,](#)  
560 [295 – 307.](#)

561 Gudmundsson, A., 1984. Formation of Dykes, Feeder-dykes, and the Intrusion of Dykes from  
562 Magma Chambers. Bulletin of Volcanology 47 (3), 537 - 550.

563 Gudmundsson, A., 1999. Fluid overpressure and stress drop in fault zones. Geophysical Research  
564 Letters 26 (1), 115 – 118.

565 [Gudmundsson, A., 2009. Toughness and failure of volcanic edifices. Tectonophysics 471, 27 –](#)  
566 [35.](#)

567 [Gudmundsson, A., 2011. Rock Fractures in Geological Processes. Cambridge University Press,](#)  
568 [pp.592.](#)

569 Gudmundsson, A. Marinoni, L. B., and Marti, J., 1999, Injection and arrest of dykes: Implications  
570 for volcanic hazards. Journal of Volcanology Geothermal Research 88, 1 - 13.

571 Gurney, J. J., and Kirkley, M. B., 1996. Kimberlite dyke mining in South Africa. *Africa*  
572 *Geoscience Review* 3, 191 - 201.

573 Hamilton, M. A., Pearson, D. G., Thompson, R. N., Kelley, S. P., and Emeleus, C. H., 1998.  
574 Rapid eruption of Skye lavas inferred from precise UPb and ArAr dating of the Rum and Cuillin  
575 plutonic complexes. *Nature* 394, 260 - 263.

576 Jaupart, C., and Allègre, C. J., 1991. Gas content, eruption rate and instabilities of eruption  
577 regime in silicic volcanoes. *Earth and Planetary Science Letters* 102, 413 - 429.

578 Kavanagh, J., 2010. Ascent and emplacement of kimberlite magmas, PhD Thesis, University of  
579 Bristol.

580 Kavanagh J., and Sparks, R. S. J., 2011. Insights of dyke emplacement mechanics from detailed  
581 3D dyke thickness datasets. *Journal of the Geological Society of London* 168, [965 – 978](#).

582 Kerr, R. C., and Lister, J. R., 1995. The lateral intrusion of silicic magmas into unconsolidated  
583 sediments: the Tennant Creek prophyry revisited. *Australian Journal of Earth Sciences* 42, 223 -  
584 224.

585 Khazanehdari, J., and Sothcott, J., 2003. Variation in dynamic elastic shear modulus of sandstone  
586 upon fluid saturation and substitution. *Geophysics* 68 (2), 472 - 481.

587 Landau, L. D., and Lifshitz, E. M., 1986. *Theory of Elasticity*, 3rd edition. Butterworth  
588 Heinemann, Oxford, England.

589 Lister, J. R., and Kerr, R. C., 1991. Steady solutions for feeder dykes in a density-stratified  
590 lithosphere. *Journal of Geophysical Research* 96, (B6), 10049 - 10077.

591 McLeod, P., and Tait, S., 1999. The growth of dykes from magma chambers. *Journal of*  
592 *Volcanology and Geothermal Research* 92, 231–245

593 Menand, T., Daniels, K. A., and Benghiat, P., 2010. Dyke propagation and sill formation in a  
594 compressive tectonic environment. *Journal Geophysical Research* 115 (B08201).

595 Menand, T., and Tait, S. R., 2002. The propagation of a buoyant liquid-filled fissure from a  
596 source under constant pressure: An experimental approach. *Journal of Geophysical Research* 107  
597 (B11), 2306.

598 Menand, T., and Tait, S. R., 2001. A phenomenological model for precursor volcanic eruptions.  
599 *Nature* 411, 678-680.

600 Meriaux. C., and Lister, J. R., 2002. Calculation of dike trajectories from volcanic centres.  
601 *Journal of Geophysical Research* 107 (B4), 2077.

602 Nicoll, G. R., Holness, M. B., Troll, V. R., Donaldson, C. H., Holohan, E. P., Emeleus, C. H.,  
603 and Chew, D., 2009. Early mafic magmatism and crustal anatexis on the Isle of Rum: evidence  
604 from the Am M'am intrusion breccia. *Geological Magazine* 146 (3), 368–381.

605 [Phillips, D. 1991. Argon isotope and halogen chemistry of phlogopite from South African  
606 kimberlites: a combined step-heating, laser probe, electron microprobe and TEM study. \*Chemical  
607 Geology: Isotope Geoscience Section\*, 87, 71–98.](#)

608 Pinel, V., and Jaupart, C., 2000. The effect of edifice load on magma ascent beneath a volcano.  
609 *Philosophical Transactions of the Royal Society of London A* 358, 1515 - 1532.

610 Pinel, V., and Jaupart, C., 2003. Magma chamber behaviour beneath a volcanic edifice. *Journal  
611 of Geophysical Research* 108 (B2), 2072.

612 Pinel, V., and Jaupart, C., 2004. Magma storage and horizontal dyke injection beneath a volcanic  
613 edifice. *Earth and Planetary Science Letters* 221, 245 - 262.

614 Poland, M., Moats, W. P., and Fink, J. H., 2008. A model for radial dike emplacement in  
615 composite cones based on observations from Summer Coon volcano, Colorado, USA. *Bulletin of*  
616 *Volcanology* 70, 861-875.

617 Pollard, D. D., 1987. Elementary fracture mechanics applied to the structural interpretation of  
618 dykes; in *Mafic dyke swarms*, Editors: Halls, H. C., and Fahrig, W. F., Geological Association of  
619 Canada Special Paper 34, 5-24.

620 Pollard, D. D., and Muller, O. H., 1976. The effect of gradients in regional stress and magma  
621 pressure on the form of sheet intrusions in cross section. *Journal of Geophysical Research* 81, (5),  
622 975 - 984.

623 [Pollard, D. D., Segall, P. and Delaney, P. T., 1982. Formation and interpretation of dilatant  
624 echelon cracks. \*Geological Society of America Bulletin\*, 93, 1291-1303.](#)

625 [Ray, R. Hetu, C. S., and Jyotirmoy, M., 2007. Structure and emplacement of the Nandurbar–  
626 Dhule mafic dyke swarm, Deccan Traps, and the tectonomagmatic evolution of flood basalts.  
627 \*Bulletin of Volcanology\* 69, 537 – 551.](#)

628 Reches, Z., and Fink, J., 1988. The mechanism of intrusion of the Inyo Dike, Long Valley  
629 Caldera, California. *Journal of Geophysical Research* 93 (B5), 4321 – 4334.

630 Roman, D. C., and Cashman, K. V., 2006. The origin of volcano-tectonic earthquake swarms.  
631 *Geology* 34 (6), 457 - 460.

632 Rubin, A. M., 1993. Tensile fracture of rocks at high confining pressure: Implications for dike  
633 propagation. *Journal of Geophysical Research* 98 (B9), 15,919 – 15,935.

634 Rubin, A. M., 1995. Propagation of magma-filled cracks. *Annual Reviews in Earth and Planetary*  
635 *Science* 23, 287 - 336.

636 Rubin, A. M., and Pollard, D. D., 1987. Origins of blade-like dikes in volcanic rift zones, in:  
637 Decker, R. W., Wright, T. L., and Stauffer, P. H., eds., *Volcanism in Hawaii*. U.S. Geological  
638 Survey professional paper 1350, 1449-1470.

639 [Tada, H., Paris, P. C., and Irwin, G. R., 2000. \*The Stress Analysis of Cracks Handbook\*, 3rd ed.,](#)  
640 [New York : ASME Press.](#)

641 Timoshenko, S. P., and Goodier, J. N., 1970. *Theory of elasticity*. McGraw-Hill, 3<sup>rd</sup> edition, pp.1-  
642 567.

643 [Schmidt, R.A. and Huddle, C.W., 1977. Effect of confining pressure on fracture toughness of](#)  
644 [Indiana limestone. \*International Journal of Rock Mechanics & Mining Sciences Geomechanics\*](#)  
645 [Abstracts 14, 289 - 293.](#)

646 Schofield, N., Stevenson, C., and Reston, T., 2010. Magma fingers and host rock fluidization in  
647 the emplacement of sills. *Geology* 38, 63 - 66.

648 Sneddon, I. N., 1946. The distribution of stress in the neighborhood of a crack in an elastic solid.  
649 *Proceedings of the Royal Society of London A* 187, 229 - 260.

650 Stasiuk, M. V., Jaupart, C., and Sparks, R. S. J., 1993. Influence of cooling on lava-flow  
651 dynamics. *Geology* 21 (4), 335 - 338.

652 Valentine, G. A., and Krogh, K. E. C., 2006. Emplacement of shallow dikes and sills beneath a  
653 small basaltic volcanic center: The role of pre-existing structure (Paiute Ridge, southern Nevada,  
654 USA). *Earth and Planetary Science Letters* 246, 217 - 230.

655 [White, R.S., Drew, J., Martens, H.R., Key, J., Soosalu, H. and Jakobsdóttir, S.S, 2011.](#)  
656 [Dynamics of dyke intrusion in the mid-crust of Iceland. \*Earth and Planetary Science Letters\*](#)  
657 [304, 300 - 312.](#)

658 Worthington, M. H., and Lubbe, R., 2007. The scaling of fracture compliance. Geological  
659 Society, London, Special Publications 270, 73 – 82.

660

661 **Table caption:**

662 Table 1: Estimated values for driving pressure ( $P_o - S_{3o}$ ) and stress gradient ( $\nabla P - \nabla S_y$ ) for Rum  
663 and Swartruggens dikes (this study), non-feeder dikes at Miyakejima volcano (Geshi et al. 2010),  
664 silicic dikes at Summer Coon volcano (Poland et al. 2008) and Walsen Dike and Theatre Canyon  
665 Sill (Pollard and Muller 1976).

666

667 **Figure captions**

668 Figure 1: The locations of the measured dikes. A generalised geological map of the isle of Rum  
669 with each of the dike measurement localities highlighted.

670

671 Figure 2: Photographs and sketches of Rum dikes. A) Plan-view of dike with crack tips showing  
672 pronounced chilled margins. One crack tip shows infilling with sediment. There is overlap  
673 between dike segments, one segment shows an apparent skew. B) Dike orientation unaffected by  
674 secondary jointing. C) Joint affected dike orientation.

675

676 Figure 3: A) Surface outcrop map of the John and Edward kimberlite dike segments, Helam  
677 Mine, South Africa. B) Contour plot of dike thickness for the John and Edward dike segments  
678 plotted against depth below the current surface and distance easting. The shaded area indicates  
679 locations where data has been collected. The approximate stratigraphy and unit contacts (dashed

680 line) are shown, comprising quartzite (Qtz), shale (Sh) and dolerite (Dol). The map inset  
681 indicates the location of Helam Mine in southern Africa (lat -25.594°, lon 26.659°).

682

683 Figure 4: Thickness versus length profile of Rum (Figures 3A, C and D) and Swartruggens  
684 (John's dike segment, 18th Level) (Figure 3B) dikes. A best-fit model (line) is plotted through  
685 the data (diamonds). Both datasets show asymmetrical dike-thicknesses, with fatter edges and  
686 thinner middles compared to the elastic model. Best-fit model parameter values are: A), C) and  
687 D)  $G = 15.4 \text{ GPa}$  (Khazanehdari and Sothcott, 2003),  $\nu = 0.215$  (Domenico, 1983),  $\Delta P = 367$   
688  $\text{MPa}$ , and  $\nabla P = 48 \text{ MPa m}^{-1}$ . B)  $G = 40 \text{ GPa}$ ,  $\Delta P = 34 \text{ MPa}$  and  $\nabla P = 65 \text{ kPa m}^{-1}$ .  $L^*$  is the along-  
689 dike distance normalised by the dike length and  $T^*$  is the half-thickness normalised by the dike  
690 length.

691

692 Figure 5: A) to D)  $T$  is dike thickness. The line at  $y=0$  is a perfect model fit to the data. Negative  
693  $y$ -axis values indicate a dike that is fatter than the model, positive  $y$ -axis values show a thinner  
694 dike than the model. Positive values are in the downwards direction. Both A) and C) the Rum  
695 dikes and B) and D) the Swartruggens dikes (John segment, Levels 16-21, and Edward segment  
696 Levels 19-22) have fatter edges and thinner centres than is expected from the model fit. Figure  
697 4C) and D) as 4A) and B), but with the vertical axis changed to show the range of -2 to 2 in order  
698 to more clearly see the distribution of the points above and below the perfect model fit (red) line.  
699 It can be seen that for both field localities, the majority of the points in the central region ( $L^* = -$   
700  $0.3$  to  $0.3$ ) show thicknesses which are narrower than expected, and at the edges ( $L^* < -0.3$  and  
701  $> 0.3$ ) the thicknesses are larger than expected. Frequency histograms of the difference between  
702 the modelled  $T$  and the measured  $T$  for E) the Rum and F) Swartruggens dikes showing the

703 distribution of data relative to 0 (the perfect model fit) for the central region of each dike (red)  
704 and the edges of each dike (black).

705

706 Figure 6: A and B) The relationship between dike tips of segmented and non-segmented dikes.

707 A) The tip of a dike with no neighboring dikes or dike segments (Rum). B) The overlapping dike  
708 tips of two segmented dikes observed at locality 5 on Rum. The dike tips are separated at this  
709 locality by approximately 10 cm.

710

711 Figure 7: A) Schematic diagram of a segmented dike. All the segments are identical, collinear,  
712 equally spaced, and loaded with the same overpressure. Two segments are represented here, but  
713 the analysis considers an infinite number of segments. B) Along-strike opening of the dike  
714 segments. The along-strike position  $x$ , measured from the segment center, is normalized to the  
715 segment half-length  $a$ , and the segment opening  $u_s$  to the maximum opening,  $\Delta P(1-\nu)a/G$ , of a  
716 single dike with the same half-length and overpressure  $\Delta P$ . The tip-to-tip distance  $d$  between  
717 adjacent dike segments is normalized to the length of the segments:  $s = d/2a$ . Only half of the  
718 segment length is shown ( $0 < L^* < 0.5$ ). The continuous curve corresponds to the case of a single  
719 dike, and the dashed curves to different normalized spacings  $s$ .

720

721 Figure 8: Opening profiles of two segments belonging to the same dike from the Isle of Rum  
722 (diamonds) compared with the segmented analysis (equation 3; black curve) and the analysis of  
723 Pollard and Muller (1976; dashed curve). A) Best overpressure estimates: 110 MPa (black curve)  
724 and 332 MPa (dashed curve). There is no stress gradient. B) Best overpressure estimates: 73  
725 MPa (black curve) and 150 MPa (dashed curve). The segmented analysis cannot explain the

726 teardrop shape of this segment. Best stress gradient estimated from Pollard and Muller's analysis  
727 (dashed curve): 136 MPa/m.

728

729 Figure 9: Schematic illustration of the impact of cooling on preserved dike geometry, presented  
730 as three time steps in the evolution of a horizontal section through the dike. A) Magma intrudes  
731 a fracture, and B) cooling ensues at the dike margins. C) Chilled fracture tip magma props the  
732 fracture open as the overpressure reduces, preventing crack closure and creating the observed  
733 dike profile (solid line) with a thinner center and thicker tips. The dashed line in C) indicates the  
734 expected profile of a pressurized magma-filled fracture in an elastic media.

735

**Table1\_Daniels**

<i>Intrusive Body</i>	<i>Number of observations</i>	<i><math>P_o - S_{yo}</math> (MPa)</i>
Rum dikes	784	37 – 1990
Swartruggens dikes	1387	4 – 40
Miyakejima volcano	>88	7 – 12
Summer Coon volcano	238	4.6 – 148.3
Walsen Dike	256	0.35 – 4.8
Theatre Canyon Sill	44	3.6 – 50

---

$\nabla P - \nabla S_y$  (kPa m<sup>-1</sup>)

---

0 – 3 x 10<sup>6</sup>

15 – 87

---

0.003 – 0.133

-0.052 – -0.71

-8.4 – -12

---

**Figure1\_Daniels**

[Click here to download Figure: FIGURE1\\_Daniels.pdf](#)

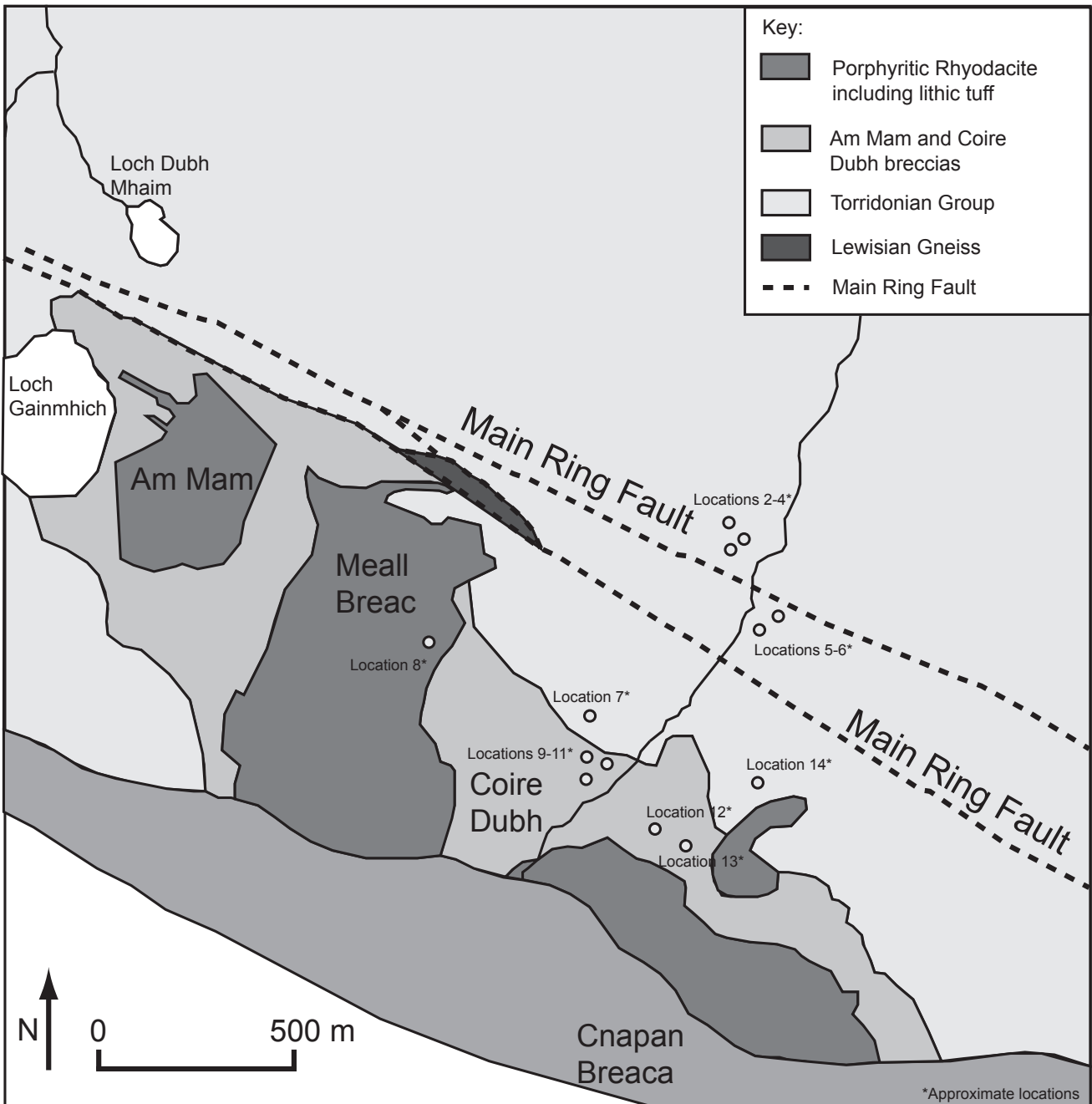
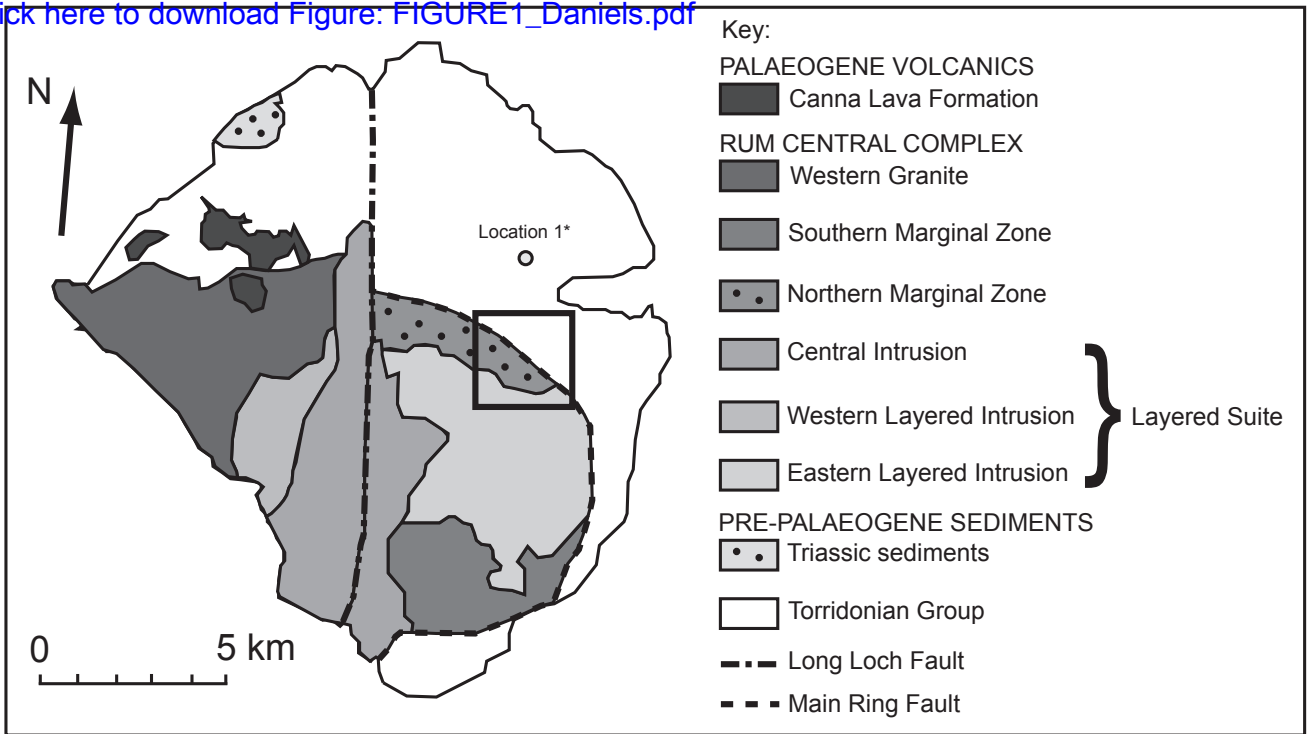
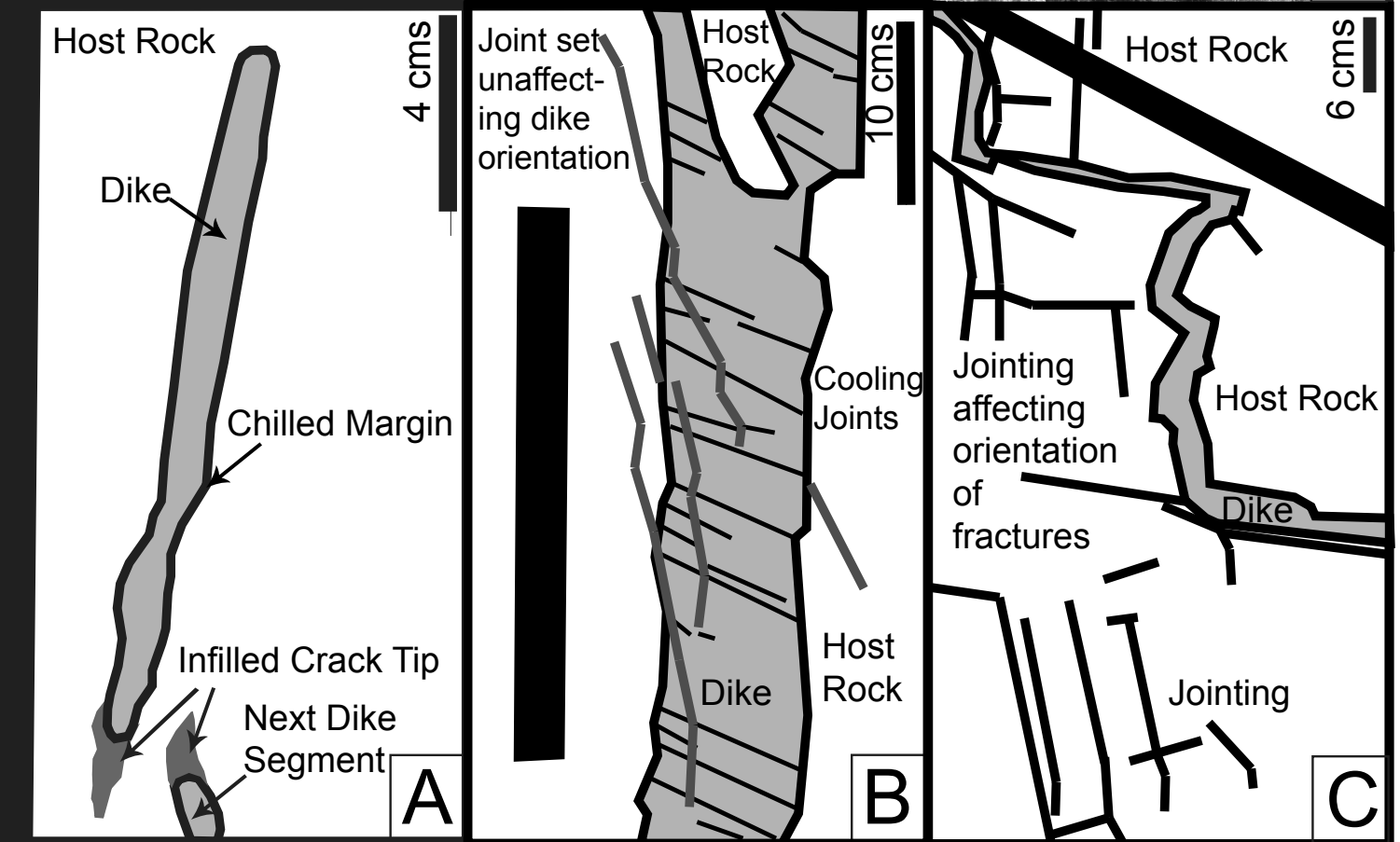
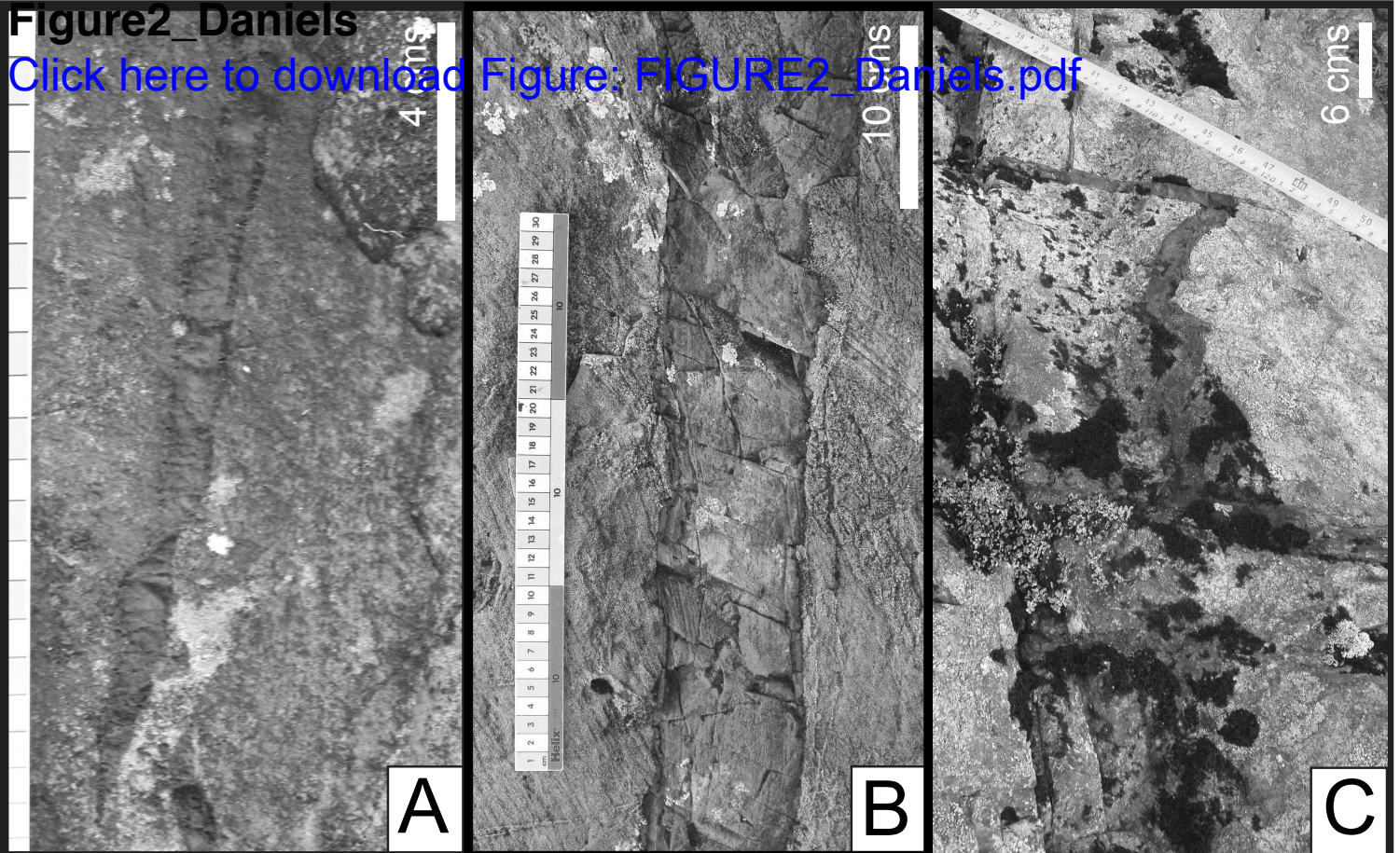
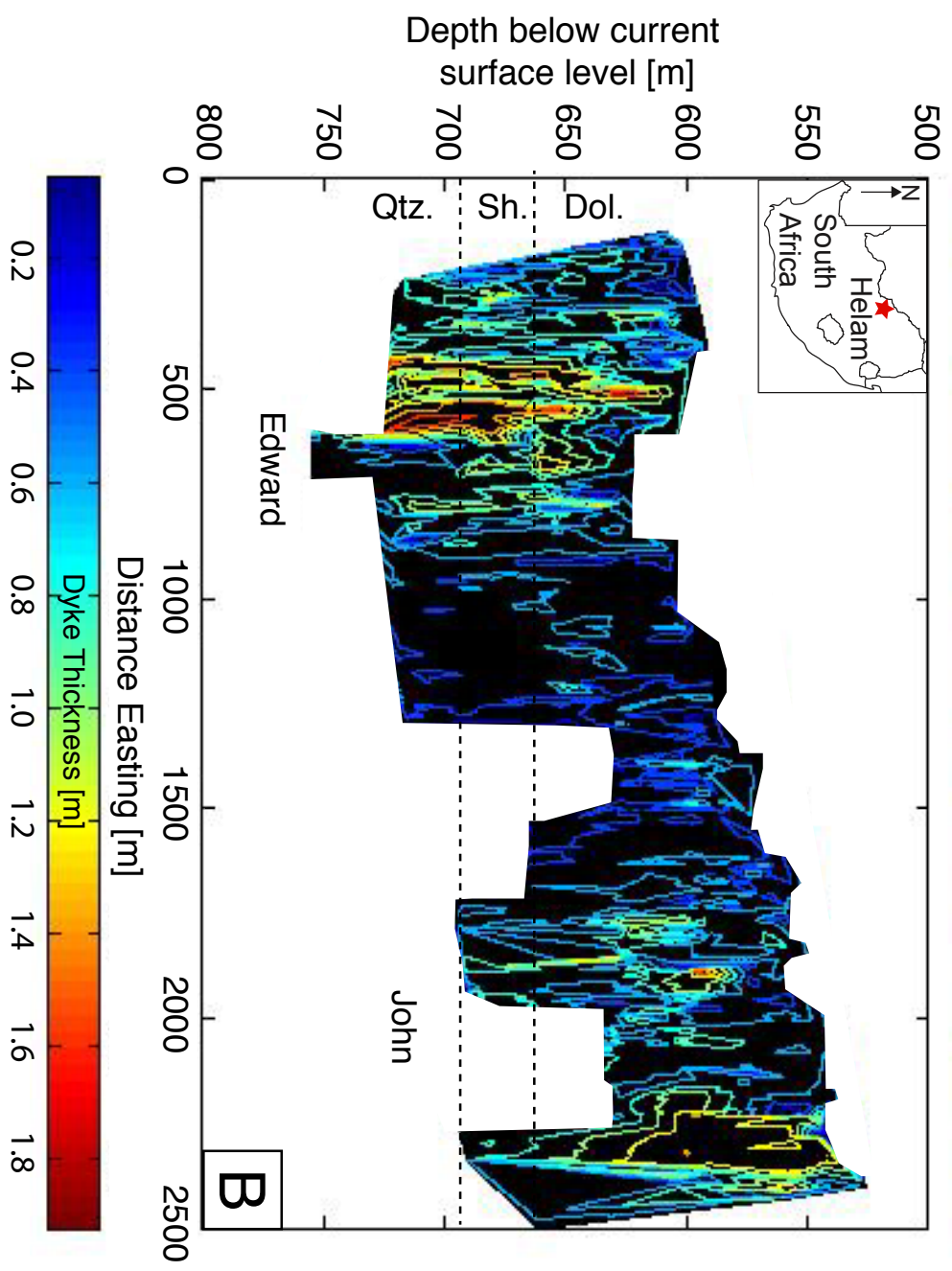
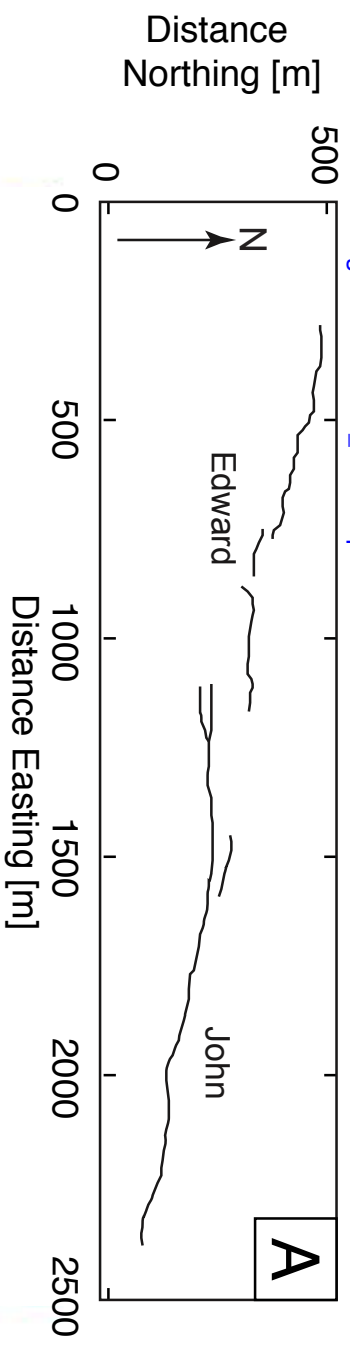


Figure2\_Daniels

[Click here to download Figure: FIGURE2\\_Daniels.pdf](#)



Figures3\_Daniels  
[Click here to download Figure: FIGURE3\\_Daniels.pdf](#)



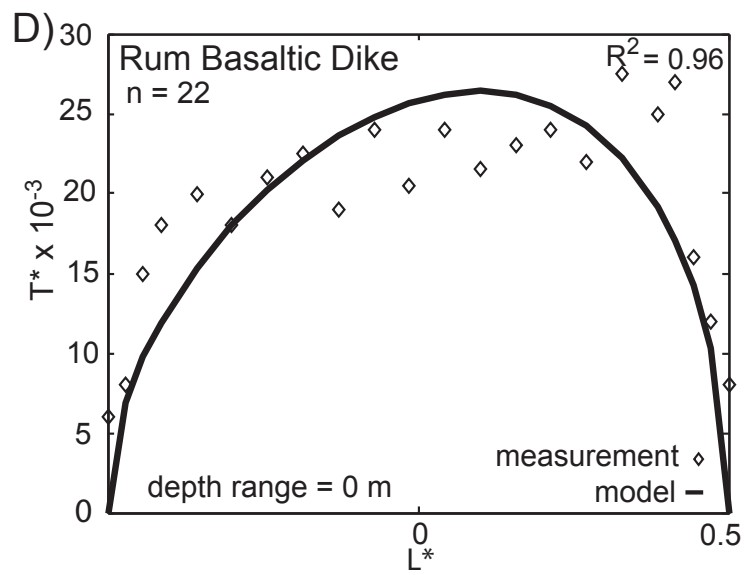
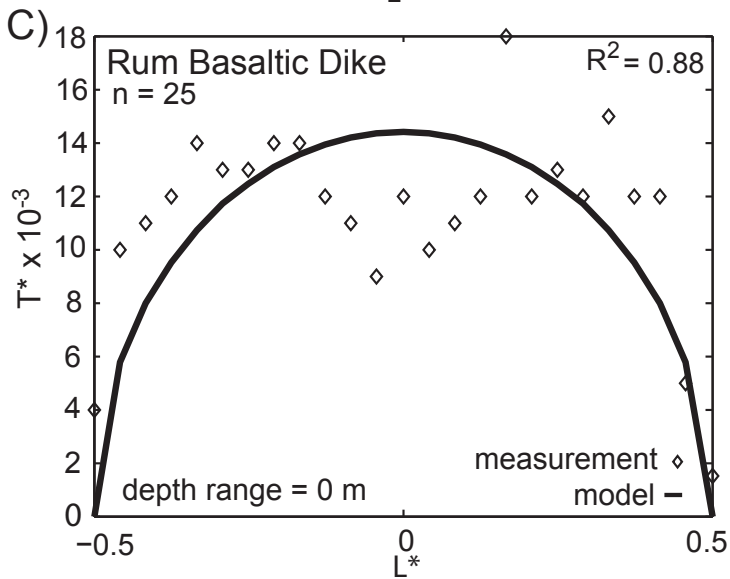
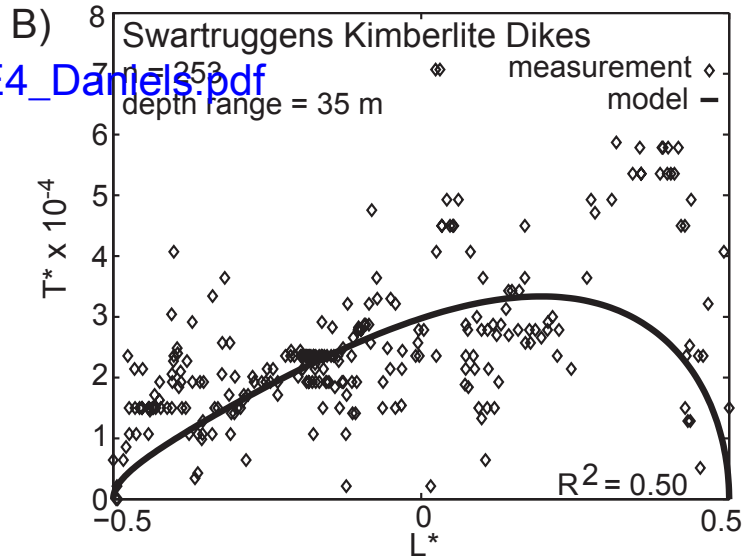
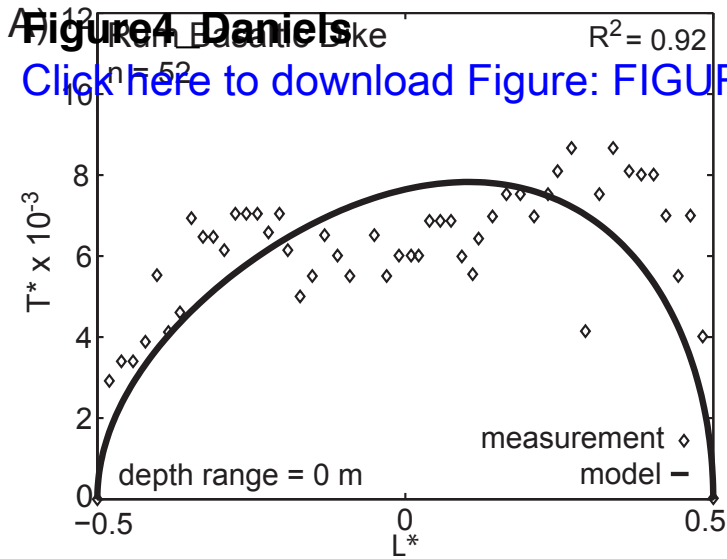
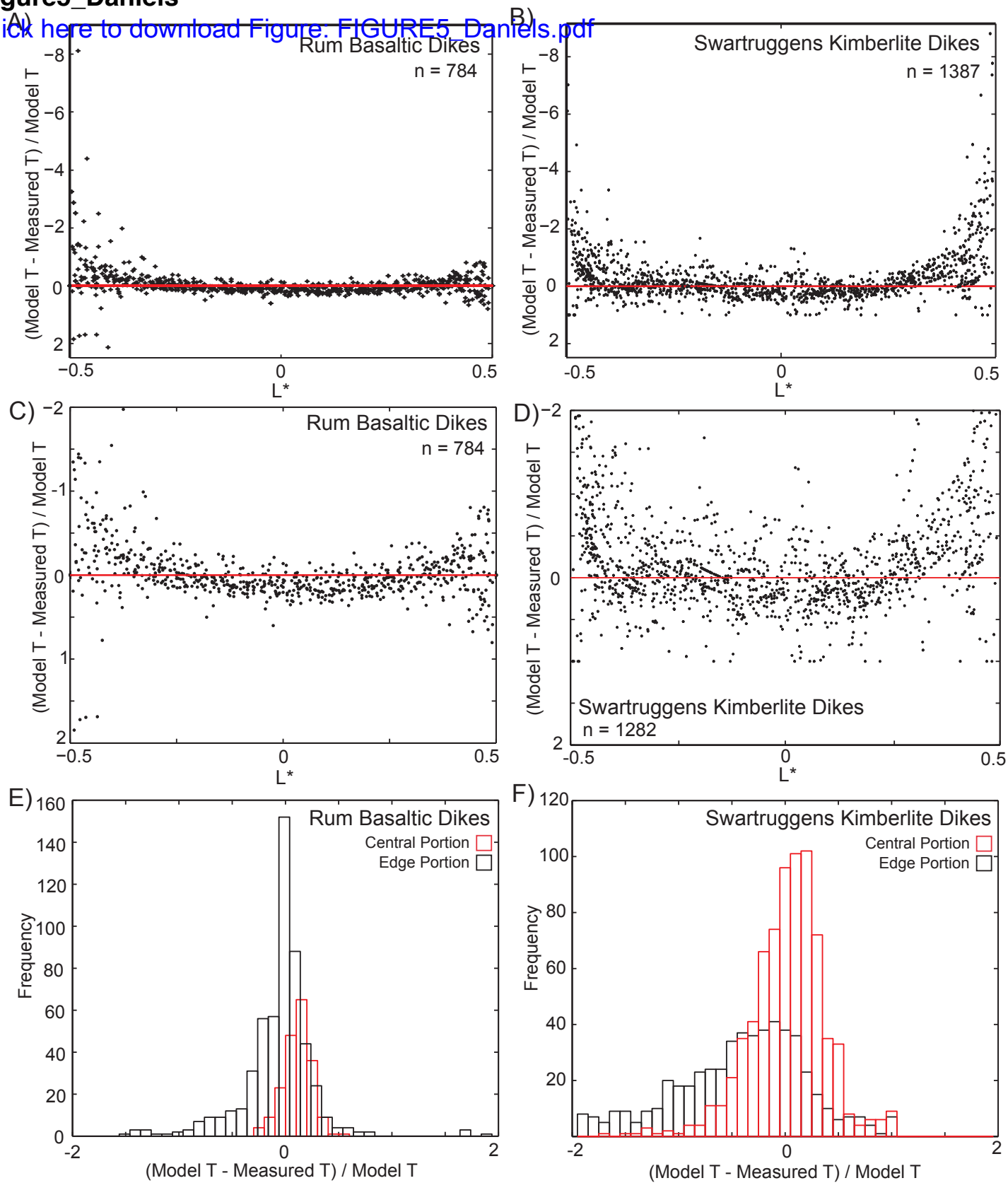


Figure4\_Daniels  
[Click here to download Figure: FIGURE4\\_Daniels.pdf](#)

**Figure5\_Daniels**

[Click here to download Figure: FIGURE5\\_Daniels.pdf](#)



# Figure6\_Daniels

[Click here to download Figure: FIGURE6\\_Dar](#)

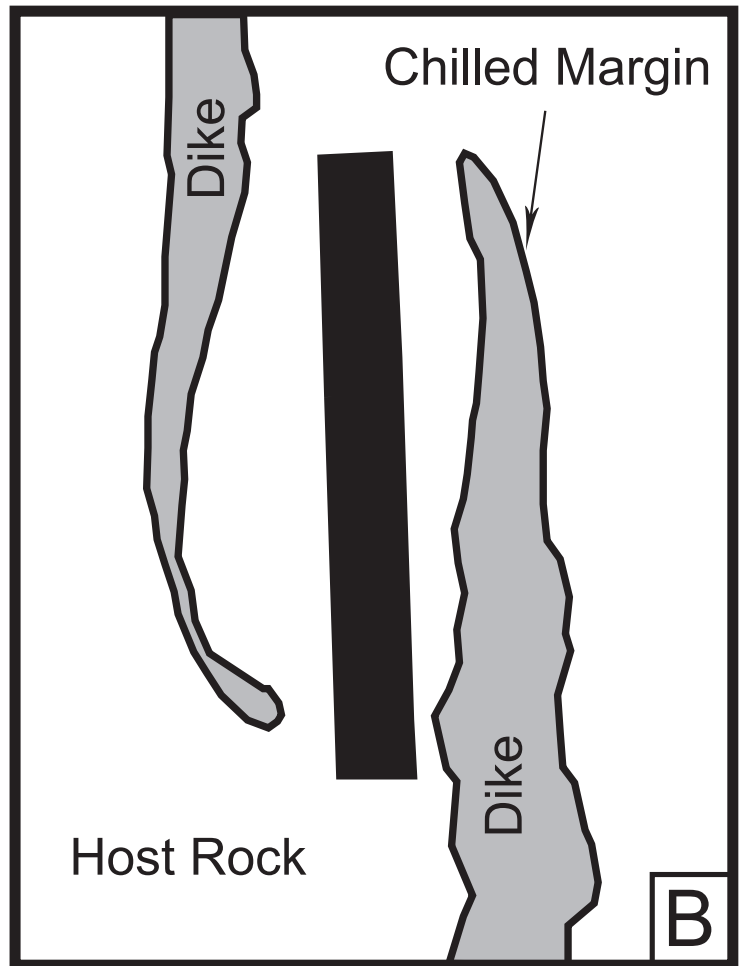
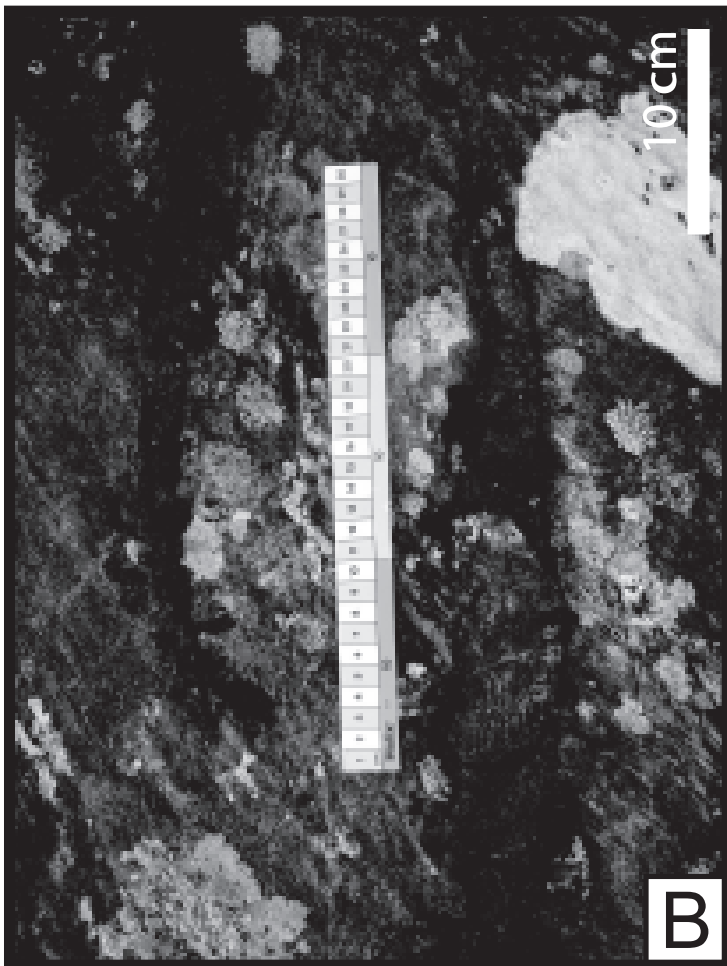
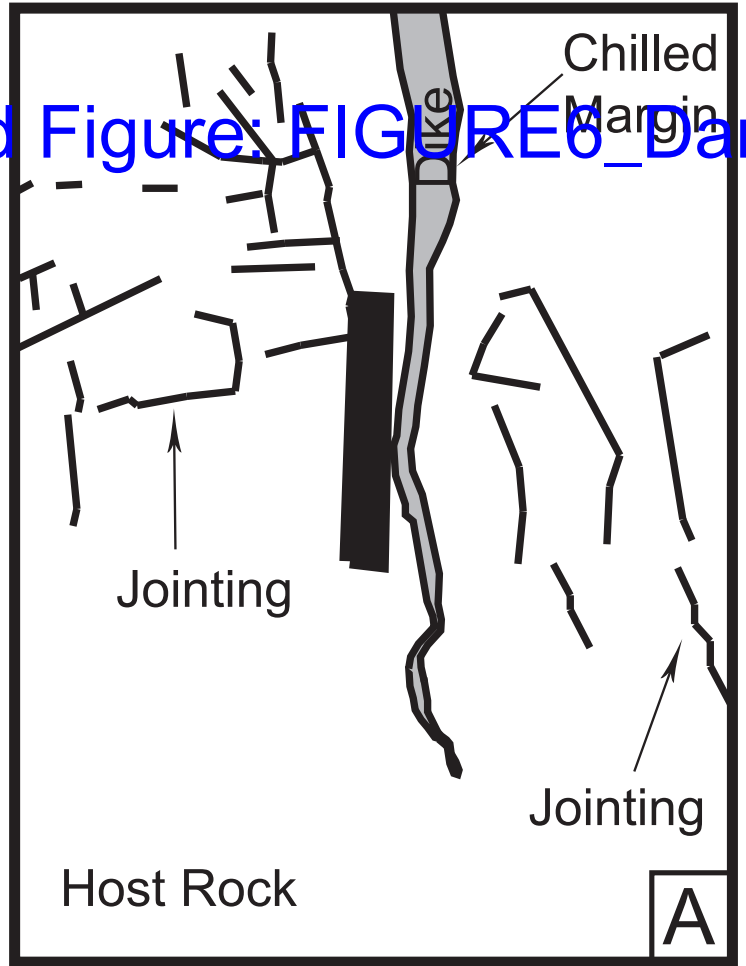
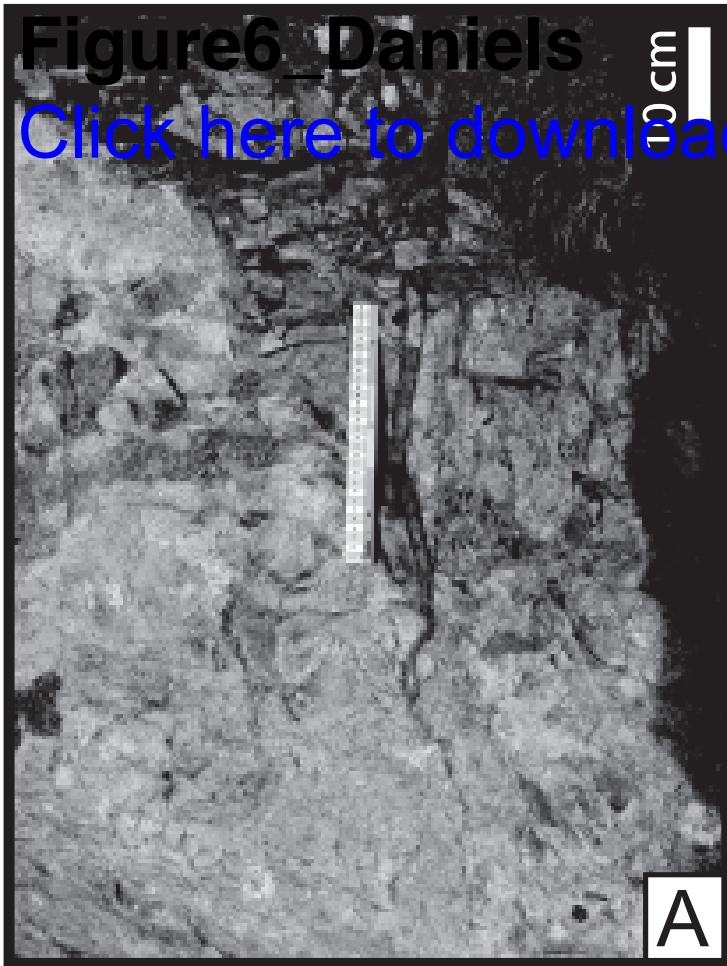


Figure7\_Daniels

[Click here to download Figure: FIGURE7\\_Daniels.pdf](#)

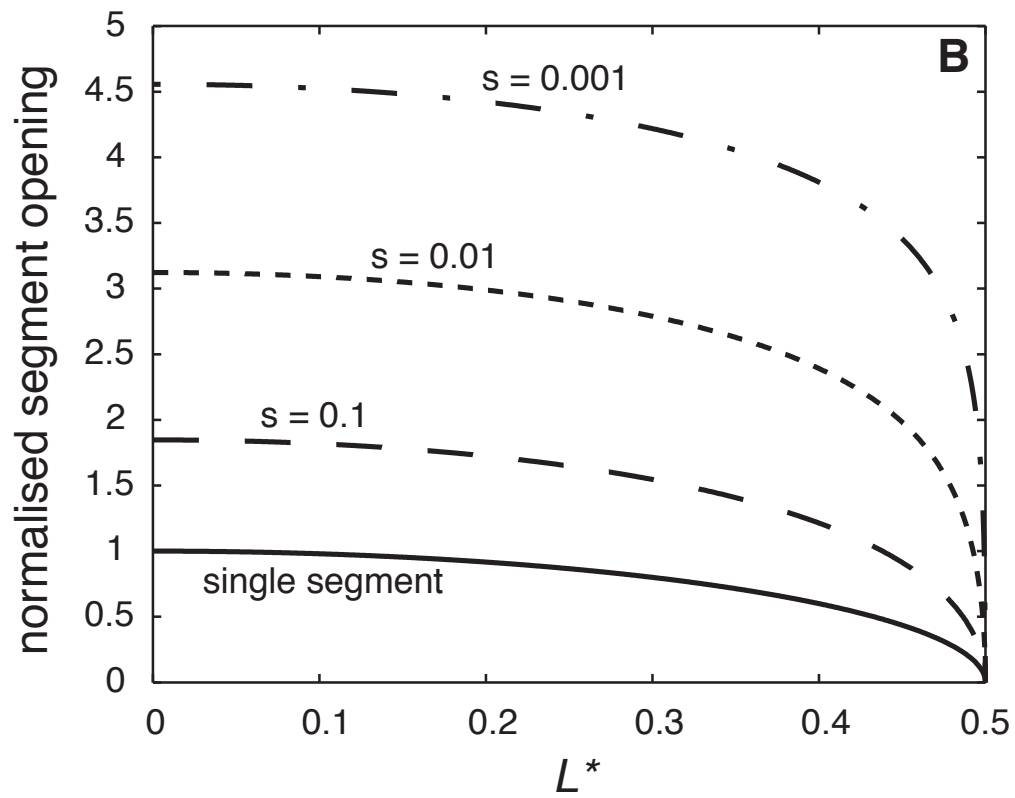
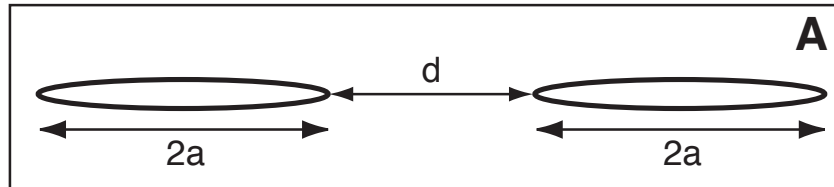
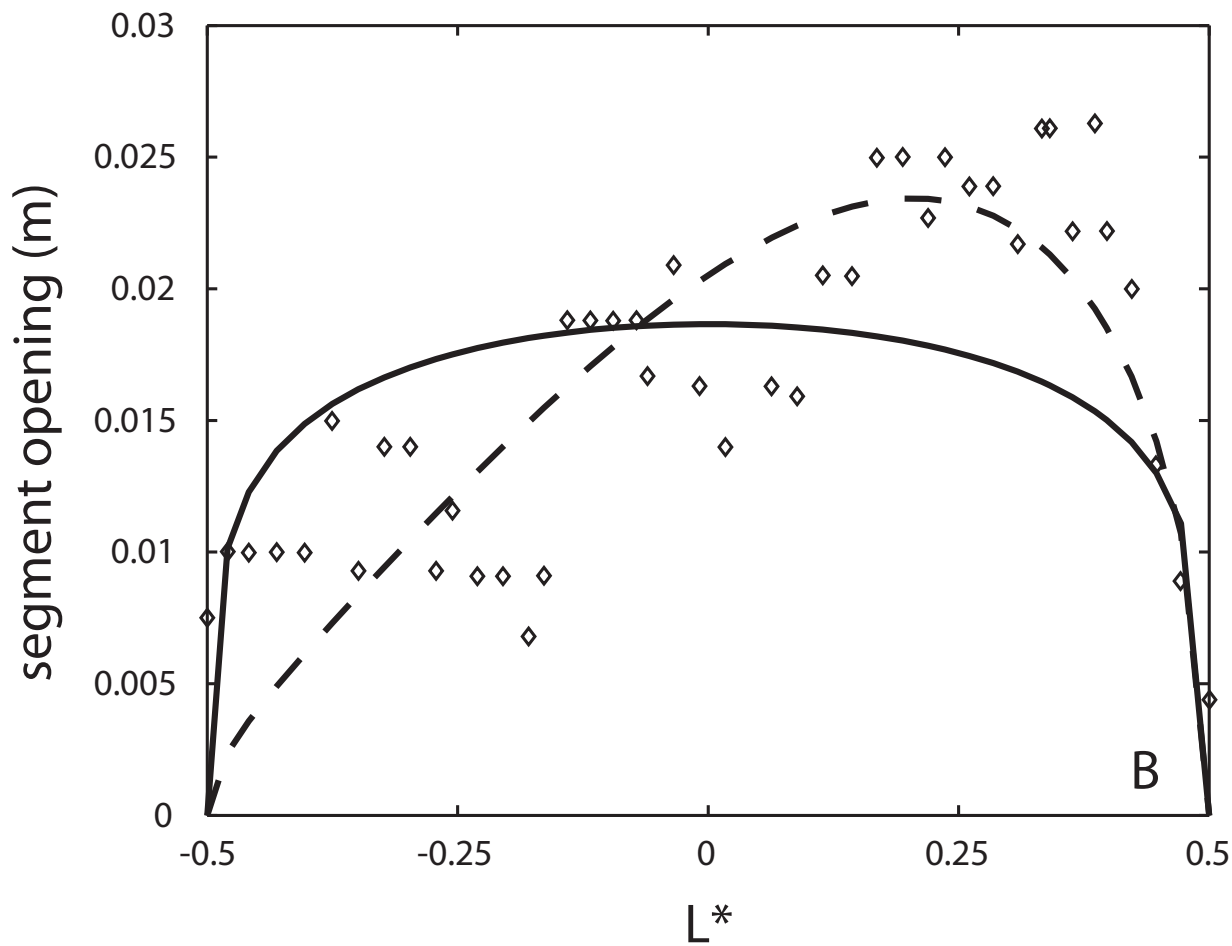
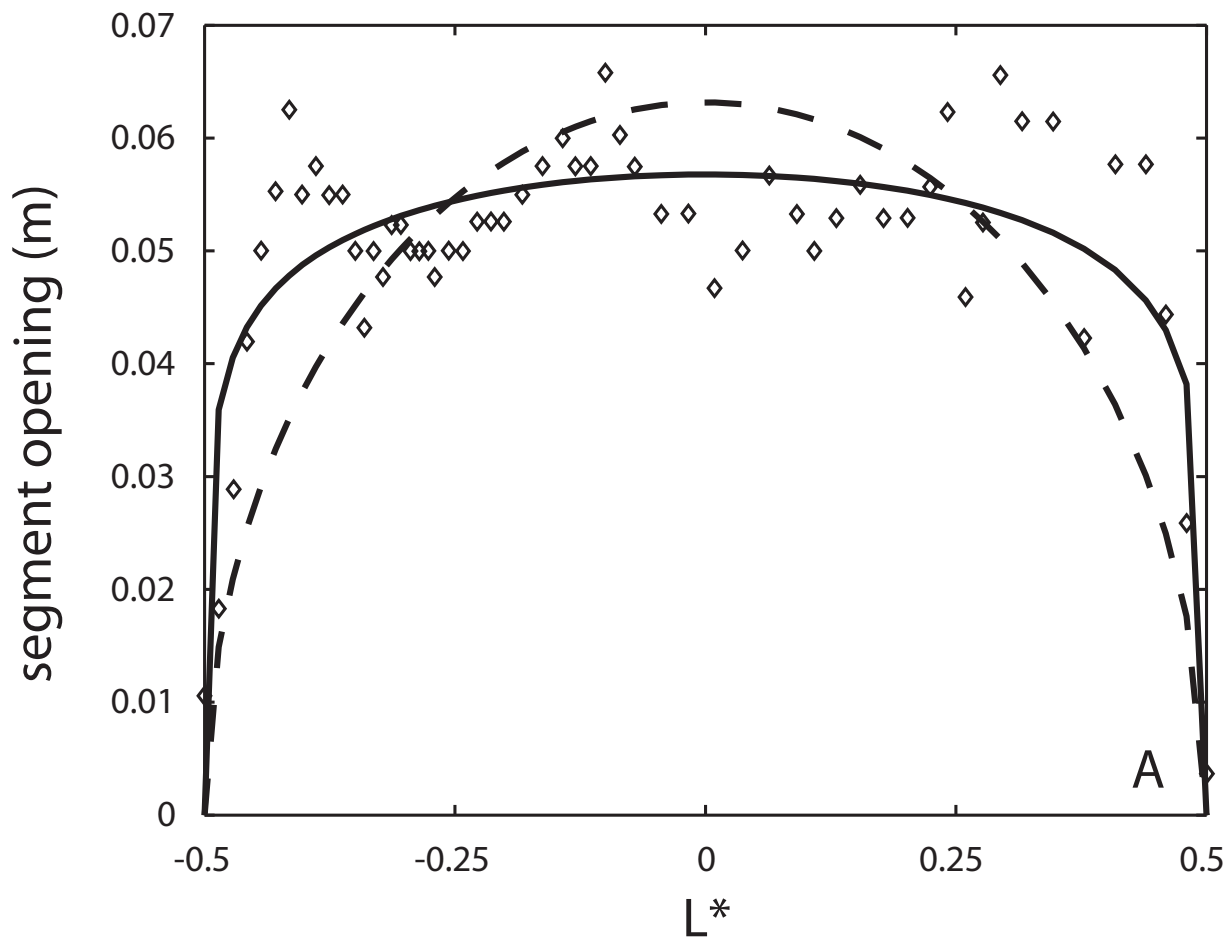


Figure8\_Daniels

[Click here to download Figure: FIGURE8\\_Daniels.pdf](#)



# Figure 9- Daniels

[Click here to download Figure:](#)

B) Chilled crack tips



C) Solidified magma in fracture

